Enzyme-constrained models and omics analysis of Streptomyces coelicolor reveal metabolic changes that enhance heterologous production

Snorre Sulheim[1,2], Tjaša Kumelj[2], Dino van Dissel[1], Ali Salehzadeh-Yazdi[3], Chao Du[4], Gilles P. van Wezel[4], Kay Nieselt[5], Eivind Almaas[2,6], Alexander Wentzel[1], Eduard J Kerkhoven[7,8,*]

1. Department of Biotechnology and Nanomedicine, SINTEF Industry, Trondheim, Norway
2. Network Systems Biology Group, Department of Biotechnology and Food Science, NTNU - Norwegian University of Science and Technology, Trondheim, Norway
3. Department of Systems Biology and Bioinformatics, Faculty of Computer Science and Electrical Engineering, University of Rostock, Rostock, Germany
4. Microbial Biotechnology, Institute of Biology, Leiden University, Leiden, The Netherlands
5. Integrative transcriptomics, Center for Bioinformatics, University of Tübingen, Tübingen, Germany

6. K.G. Jebsen Center for Genetic Epidemiology, Department of Public Health and General Practice, NTNU - Norwegian University of Science and Technology, Trondheim, Norway
7. Systems and Synthetic Biology, Department of Biology and Biological Engineering, Chalmers University of Technology, Gothenburg, Sweden
8. Novo Nordisk Foundation Center for Biosustainability, Chalmers University of Technology, Gothenburg, Sweden

∗ Corresponding author and Lead Contact. Email: eduardk@chalmers.se

Abstract

Many biosynthetic gene clusters (BGCs) require heterologous expression to realize their genetic potential, including silent and metagenomic BGCs. Although the engineered *Streptomyces coelicolor* M1152 is a widely used host for heterologous expression of BGCs, a systemic understanding of how its genetic modifications affect the metabolism is lacking and limiting further development. We performed a comparative analysis of M1152 and its ancestor M145, connecting information from proteomics, transcriptomics, and cultivation data into a comprehensive picture of the metabolic differences between these strains. Instrumental to this comparison was the application of an improved consensus genome-scale metabolic model (GEM) of *S. coelicolor*. Although many metabolic patterns are retained in M1152, we find that this strain suffers from oxidative stress, possibly caused by increased oxidative metabolism. Furthermore, precursor availability is likely not limiting polyketide production, implying that other strategies could be beneficial for further development of *S. coelicolor* for heterologous production of novel compounds.

40 ## Introduction

41 The bacterium *Streptomyces coelicolor* has been the *de facto* model actinomycete for the
42 production of antibiotics. Being known for over 100 years, the interest in this organism
43 predates the golden age of antibiotic research. With its complex life cycle, featuring mycelial
44 growth and differentiation, spore formation, programmed cell death and the ability to
45 produce multiple coloured secondary metabolites it has assisted greatly in our
46 understanding of how streptomycetes sense their surrounding (Hahn, Oh, and Roe 2002;
47 Hutchings et al. 2004; Nothaft et al. 2010, 2; Rigali et al. 2008; Sola-Landa et al. 2005),
48 activate their developmental cycle (Chandra and Chater 2014) and regulate the production
49 of antibiotics (Nieselt et al. 2010; Thomas et al. 2012). Further aided by the publication of its
50 genome sequence (Bentley et al. 2002), the antibiotic coelimycin P1 (yellow), produced from
51 the formerly cryptic polyketide gene cluster known as *cpk*, was added to this list (Gomez-
52 Escribano et al. 2012). Today, the widespread use of *S. coelicolor* continues as a host for
53 heterologous production of biosynthetic gene clusters (BGCs) (Castro et al. 2015; Gomez-
54 Escribano and Bibb 2011; 2014; Kumelj et al. 2018; Thanapipatsiri et al. 2015; Yin et al.
55 2015). Heterologous expression is a powerful strategy for novel compound discovery from
56 BGCs that are either natively silent or originate from an unculturable source (Nepal and
57 Wang 2019). These BGCs represent an untapped resource of microbial biodiversity,
58 nowadays made evident and accessible due to recent advances within the fields of
59 metagenomics, molecular biology and bioinformatics (Rutledge and Challis 2015).

60 The efficiency of *S. coelicolor* as a heterologous production host relies on a metabolism that
61 has evolved to provide the necessary precursors to produce a broad range of complex
62 molecules. Many of these molecules are produced when the strain is experiencing nutrient-

limiting conditions that lead to growth cessation and complex re-modelling of its metabolism (Wentzel, Bruheim, et al. 2012). Metabolic switching in response to phosphate and glutamate depletion has been studied in detail at a variety of metabolic levels in *S. coelicolor* M145 (Nieselt et al. 2010; Thomas et al. 2012; Wentzel, Sletta, et al. 2012), a the most well-known wild-type strain devoid of the two plasmids SCP1 and SCP2 present in the parent strain *S. coelicolor* A3(2) (Kieser et al. 2000). This has unravelled a complex sequence of switching events that ultimately lead to the biosynthesis of calcium-dependent antibiotic (CDA), and the coloured antibiotics actinorhodin (Act, blue) and undecylprodigiosin (Red, red). The biosynthesis of coelimycin P1 occurs earlier than the three other compounds in the growth cycle and appears to be independent of the major metabolic switch (Nieselt et al. 2010).

To improve *S. coelicolor* M145 as a host for heterologous BGCs expression, strain M1146 was created by the sequential deletion of its four major BGCs (*act, red, cda* and *cpk*) (Gomez-Escribano and Bibb 2011). This should increase precursor availability for the production of a whole range of heterologous products and provides a cleaner chromatographic background to more easily identify novel compounds. *S. coelicolor* M1152 is a derivative of M1146, that besides the deletion of the four main BGCs bears the C1298T point mutation in the *rpoB* gene that encodes the beta subunit of RNA polymerase. This mutation was shown to have strong positive effects on the production of various antibiotics (Gomez-Escribano and Bibb 2011; Hu, Zhang, and Ochi 2002). Up to now, M1152 is a preferred general 'superhost' for heterologous BGC expression (Braesel, Tran, and Eustáquio 2019; Castro et al. 2015; Kepplinger et al. 2018; T. Li et al. 2013; Thanapipatsiri et al. 2015) and is the starting point for further strain development.

86

87 Previous research on the metabolism of *S. coelicolor* M1152 have been confined to
88 transcriptome profiling of batch fermentations (Battke, Symons, and Nieselt 2010; Jäger,
89 Battke, and Nieselt 2011; Liao, Smyth, and Shi 2014; Love, Huber, and Anders 2014; Mi et al.
90 2019), and further development of this strain as a 'superhost' calls for a better
91 understanding of how the genetic modifications have affected M1152s regulatory system
92 and metabolism. To this end we measure both protein and transcript levels of both M1152
93 and its parent strain, M145, at different time steps during batch fermentation where the
94 metabolic switch is triggered by depletion of phosphate. Since enzymes are catalysing most
95 metabolic transformations, assessing protein abundance provides information about the
96 metabolic capacity of the organism. Furthermore, we do not only consider the protein
97 abundances in isolation, but use these measurements to confine fluxes predicted by a
98 genome-scale metabolic model (GEM) of *S. coelicolor* to the maximum capacity of the
99 enzymes. By doing so we propagate differences in the abundance of individual enzymes in
100 M145 and M1152 to metabolic rearrangements on the systems level.

101

102 The metabolic network in the cell is described in a GEM (Gu et al. 2019). GEMs are both
103 valuable resources of strain-specific knowledge, mathematical models able to predict
104 steady-state flux distributions, and frameworks for interpretation and integration of
105 different ‘omics’ data, e.g. transcriptomics and proteomics (Robinson and Nielsen 2016). The
106 increased interest in using genome-scale models of *S. coelicolor* is conspicuous. Since the
107 first reconstruction in 2005 (Borodina, Krabben, and Nielsen 2005), five GEMs have been
108 published (Alam et al. 2010; Amara, Takano, and Breitling 2018; M. W. Kim et al. 2014;

109 Kumelj et al. 2018; Wang et al. 2018), including three in 2018: iKS1317 (Kumelj et al. 2018),
110 Sco4 (Wang et al. 2018) and iAA1259 (Amara, Takano, and Breitling 2018). Additionally, as a
111 model organism for the *Actinomycetes,* the GEMs of *S. coelicolor* are frequently used as
112 template for model development of closely related strains (Mohite et al. 2019), such as *S.*
113 *clavuligerus* (Toro et al. 2018), *Saccharopolyspora erythraea* (Licona-Cassani et al. 2012) and
114 *S. lividans* (Valverde, Gullón, and Mellado 2018). The recent updates of the *S. coelicolor* GEM
115 were developed in parallel by different research groups: while all groups share the common
116 interest of utilizing a high-quality model for predictions and data analysis, the prevailing
117 approach of independent parallel development is inefficient. Additional to duplicating a
118 considerable amount of work, lack of common standards for documentation of progress and
119 issues, evaluation of model performance, as well as the use of different annotations makes it
120 cumbersome to compare and merge models.

121 To increase the rate and quality of model reconstruction, in this study two research groups
122 of the *S. coelicolor* GEM community, responsible for two of the latest model updates (Kumelj
123 et al. 2018; Wang et al. 2018), have joined forces to merge existing GEMs of *S. coelicolor* into
124 one consensus-model that is publicly hosted on GitHub and can be continuously updated
125 and improved by all members of the community. Hosting the model on GitHub has many
126 advantages: (i) open access and contribution; (ii) version control; (iii) continuous
127 development and integrated quality control with memote (Lieven et al. 2018); (iv) new
128 improvements released instantly (no publication lag time); and (v) complete documentation
129 of model reconstruction. Such an approach has historic precedents: model reconstruction as
130 a community effort has been a success for the human GEM (Thiele et al. 2013), baker's yeast
131 (Aung, Henry, and Walker 2013; Dobson et al. 2010; Heavner et al. 2012; 2013; Herrgård et
132 al. 2008; Lu et al. 2019) and Chinese Hamster Ovary cells (Hefzi et al. 2016). The recent

133 developments in *S. coelicolor* model and strain improvements in different research groups
134 prove that it is an opportune time now to join forces in the *Streptomyces* modelling efforts
135 as well.

136 Results

137 Reconstruction of the consensus genome-scale model of *S. coelicolor*

138 We conducted a stepwise reconstruction of Sco-GEM, the consensus genome-scale
139 metabolic model of *S. coelicolor*, while tracking development using Git for version control
140 (**Figure 1A; Data Set S1, Tab 1**). Sco-GEM is the most comprehensive and highest quality
141 GEM of this organism (**Figure 1B**), comprising 1777 genes, 2612 reactions, 2073 metabolites
142 and a memote score of 77%, which is indicative of the overall model quality (Lieven et al.
143 2018). Sco-GEM features an accuracy of 96.5% and 74.5% (**Figure 1C**) in predicting correct
144 phenotypes for growth environments and knockout mutants, respectively, yielding in total a
145 Matthews Coefficient of Correlation of 0.53 with the test data previously described (Kumelj
146 et al. 2018).

147 With the recently published iKS1317 model (Kumelj et al. 2018) as a starting point, Sco-GEM
148 was first developed by including genes, reactions and metabolites from the equally recently
149 published models iAA1259 (Amara, Takano, and Breitling 2018) and Sco4 (Wang et al. 2018).
150 While the curations from iAA1259 were primarily related to coelimycin P1, butyrolactone,
151 xylan and cellulose pathways, the 377 reactions added to Sco-GEM from Sco4 were
152 scattered across a large range of different subsystems, covering both primary and secondary
153 metabolism (**Figure S1**). Subsequent to merging the existing *S. coelicolor* GEMs, we
154 performed a number of further curations of the model (**Figure 1A**): including improvement
155 of annotations, both in terms of coverage and number of different databases, e.g. KEGG (M.

156 Kanehisa 2000; Minoru Kanehisa et al. 2019), BioCyC (Karp et al. 2017), ChEBI (Hastings et al.
157 2016) and MetaNetX (Moretti et al. 2016). All reactions and metabolites have been given
158 identifiers according to the BiGG namespace (King et al. 2016), and all reactions are
159 categorized into 15 different subsystems, covering 128 different pathways.

160 The biomass composition was curated to reflect estimated levels of prosthetic groups that
161 are associated to cellular proteins. Proteomics data, as discussed below, were used to
162 estimate protein levels, while UniProt (The UniProt Consortium 2019) provided annotations
163 of proteins with prosthetic groups, which was used to estimate overall prosthetic group
164 levels (**Data Set S1, Tab 2**).

165 Reaction reversibility updated for almost a third of queried reactions

166 The determination of reaction directionality and reversibility is an important step in a GEM
167 reconstruction (Thiele and Palsson 2010). However, the thermodynamic consistency of
168 reactions was not considered in previous *S. coelicolor* models. We calculated Gibbs free
169 energy changes for 770 of the 2612 model reactions (**Data Set S1, Tab 3**) using eQuilibrator
170 (Flamholz et al. 2012), and found hardly any consistency between the calculated change in
171 Gibbs free energy and the reversibility previously assigned to the model reactions (**Figure**
172 **1D**). To address this issue we decided to reassign the reversibility of the model reactions by
173 using a relatively lenient threshold of −30 kJ/mol to classify a reaction as irreversible (Bar-
174 Even et al. 2012; Feist et al. 2007); with the intent not to over-constrain the model (**Figure**
175 **1E**). The proposed changes in reversibility were evaluated against growth and knockout data
176 (Kumelj et al. 2018), discarding 61 of the 332 proposed reactions, and consequentially, the
177 flux bounds of 271 reactions were modified (see Transparent Methods). Additionally, all
178 ATP-driven reactions were manually curated and generally assumed irreversible unless they

179 had an estimated positive change in Gibbs free energy or were known to be reversible.
180 Examples of this include nucleoside diphosphate kinase (Chakrabarty 1998) and ATP
181 synthase (Yoshida, Muneyuki, and Hisabori 2001). The manual curation of ATP-driven
182 reactions led to a change in reversibility for 56 reactions.

183 ## Curation of transport reactions

184 As transport reactions have previously not been extensively curated in *S. coelicolor* models,
185 we performed a thorough curation of transporters by querying various databases and BLAST
186 analysis as detailed in Materials and Methods. This culminated in adding 43 new transport
187 reactions and updating 39 of the 262 existing reactions in Sco-GEM (**Figure 1F; Data Set S1,**
188 **Tab 4**). The majority of the transporters comprises primary active transport proteins and
189 secondary carriers (46%), in accordance with previous work (Getsin et al. 2013). Most
190 primary active transporters are ATP-binding cassette (ABC) transporters (30%), while proton
191 symports (30%) dominate the secondary carriers.

192 ## Development of the enzyme-constrained model EcSco-GEM

193 To include explicit constraints regarding enzymes catalysing metabolic reactions, the GECKO
194 formalism (Sánchez et al. 2017) was applied to consider that catalysing capacity is
195 constrained by enzyme turnover rates (k_{cat}) and abundances. The GECKO toolbox modifies
196 the structure of an existing GEM to integrate turnover rates and proteome data.
197 Consequentially, this constrains the range of estimated fluxes to a biologically feasible range
198 as determined by the amount and efficiency of each enzyme. Note that this approach
199 regards the maximum catalytic activities but does not consider other kinetic parameters
200 such as affinity constants. The overall flux variability of the resulting enzyme-constrained
201 model (EcSco-GEM) is drastically reduced compared to the classic genome-scale model

202 (**Figure 1G**), particularly due to the considerably reduced fraction of reactions that have very
203 high (10^1) flux variability. As reactions with high variability result in low certainty in the
204 estimated fluxes, the observed reduction in flux variability is therefore a qualitative measure
205 of the increased accuracy achieved by constraining the range of possible fluxes to those
206 satisfying the limitation in protein allocation.

207 In our endeavour to describe the metabolic differences between M145 and M1152 we
208 generated in total 17 time- and strain-specific enzyme-constrained models by combining
209 EcSco-GEM with estimated growth-, secretion- and uptake rates, as well as proteome data
210 from cultivations that are detailed and analysed below.

211 Framework for further development of Sco-GEM by the community

212 The Sco-GEM model is hosted as an open repository as suggested by memote, a recently
213 developed tool for transparent and collaborative model development (Lieven et al. 2018).
214 The memote tool is incorporated in the repository through Travis CI and tracks the model
215 development on every change of the model. Sco-GEM v1.2.0 achieved a memote-score of
216 77%, which is superior to any previous model of *S. coelicolor* (**Figure 1B; Supplemental**
217 **Information**).

218 Hosting Sco-GEM on GitHub with memote integration ensures continuous quality control
219 and enables public insight into all aspects of model reconstruction and curation: any user
220 can report errors or suggest changes through issues and pull requests. As contributions to
221 the model development are fully trackable and can therefore be credited fairly, Sco-GEM is
222 positioned as a community model that we envision to be continuously updated and widely
223 used by the *S. coelicolor* research community. While the major steps of model
224 reconstruction have been detailed in the preceding sections, every detail of the process and

225 every iteration of the model is accessible on the public model repository at
226 https://github.com/SysBioChalmers/Sco-GEM.

227 In the remaining parts of the Results section, we have applied Sco-GEM along with
228 transcriptome and proteome data, to study and compare the responses of *S. coelicolor*
229 M145 and M1152 to phosphate depletion on a systems level and for the first time provide
230 detailed insight into the distinct physiological features of engineered 'superhost' strain
231 M1152, which will be of value for its further development.

232

233 Random sampling of enzyme-constrained GEMs capture metabolic rearrangements in 234 response to phosphate depletion in M145

235 To evaluate whether the (Ec)Sco-GEM models can simulate behaviours of *S. coelicolor*
236 metabolism, we analysed time-course sampled cultivations of secondary metabolite
237 producing strain M145 using the generated models. For that purpose, *S. coelicolor* M145 was
238 cultivated in batch fermentations using standardized protocols reported earlier (Wentzel,
239 Bruheim, et al. 2012). Cultures were sampled for 'omics data, as well as substrate utilization
240 and secondary metabolite measurements to identify regulatory, proteomic and metabolic
241 changes during the metabolic switch. The online and offline measurements showed that
242 phosphate depletion in the cultivation medium was reached approximately 35 hours after
243 inoculation. Shortly after, the culture growth ceased, and first Red and subsequently Act
244 were detected in the culture medium (**Figure 2A and 2B)**. Act levels were determined by
245 measuring the amount of total blue pigments (TBP) because this covers both the
246 intracellular and secreted variants of actinorhodin, and is considered to be the preferred
247 method (Wentzel, Bruheim, et al. 2012; Bystrykh et al. 1996). Both D-glucose and L-

248 glutamate were consumed concomitantly, and their consumption continued after phosphate
249 depletion, while both remained in excess until the end of cultivation. Note that *Streptomyces*
250 can utilize intracellular phosphate storages after the medium is phosphate depleted
251 (Smirnov et al. 2015). The RNA-seq and untargeted proteomic data were analysed in the
252 light of previous studies (Nieselt et al. 2010; Thomas et al. 2012) and were in good
253 agreement with data previously obtained from microarrays or targeted proteomics (Alam et
254 al. 2010; Nieselt et al. 2010) (**Figure 2C and S2**). This confirmed the high reproducibility of
255 the experiments across independent cultivations and high reliability of the chosen
256 cultivation and analytic procedures (**Figure 2**).

257 The proteome data were incorporated into EcSco-GEM to yield time-specific metabolic
258 models of M145, giving insight on the changes occurring in the metabolic activity of different
259 pathways during batch cultivation. Metabolic fluxes were estimated using an unbiased
260 approach of random sampling, as alternative to optimization of a well-defined cellular
261 objective used in flux balance analysis (Orth, Thiele, and Palsson 2010). It is possible that *S.*
262 *coelicolor* is wired to maximize its growth rate prior to phosphate depletion, but after the
263 metabolic switch, it is difficult to define a clear cellular objective. We applied an approach
264 that samples the vertices of the solution space (Bordel, Agren, and Nielsen 2010), and used
265 their mean values to compare the metabolic fluxes between the two strains and between
266 different time points. The variation in predicted fluxes through different pathways in M145 is
267 an initial validation of the approach (**Figure 2D**): the most drastic change in fluxes occur in
268 response to phosphate depletion, in agreement with observations in the transcriptome,
269 metabolome and proteome (Nieselt et al. 2010; Thomas et al. 2012; Wentzel, Sletta, et al.
270 2012).

271

272 The response to phosphate depletion from the medium is achieved by a set of genes,
273 positively regulated by PhoP, that are involved in phosphate scavenging, uptake and saving
274 (Martín et al. 2012; Martín-Martín et al. 2018; Sola-Landa, Moura, and Martín 2003). In our
275 cultivations the metabolic switch can be readily identified from the RNA-seq data by the
276 rapid upregulation of this regulon after 35 hours of cultivation in M145 (**Figure 2C**), thereby
277 corroborating the model simulations (**Figure 2D**) and providing a more detailed picture of
278 the underlying regulation. PhoP also represses nitrogen assimilation (Martín, Rodríguez-
279 García, and Liras 2017), which can partly explain the change in amino acids metabolism after
280 phosphate depletion (**Figure 2D**). Indeed, from the RNA-seq data we find that glutamate
281 import, the glutamate sensing system *gluR-gluK* (L. Li, Jiang, and Lu 2017), *glnR* (Fink et al.
282 2002) and *glnA* are downregulated immediately subsequent to phosphate depletion (**Figure**
283 **S3**). Since PhoP is also known to regulate negatively the biosynthesis of secondary
284 metabolites, the switching of its expression likely delays these pathways (Martín 2004;
285 Martín, Rodríguez-García, and Liras 2017). However, after 37 hours of cultivation the
286 upregulation of the *cda* and *red* genes was observed, whereas that of the *act* genes was
287 initiated at 41 hours (**Figure 2E**). Production of Red and Act was measurable in the culture
288 medium after 41 and 49 hours of cultivation, respectively (**Figure 2A**). The enzyme-
289 constrained models predict an immediate increase in fluxes through the biosynthetic
290 pathways for the four main compounds Act, Red, CDA and coelimycin P1 after the metabolic
291 switch (**Figure 2D**).

292

293 The onset of secondary metabolism is strongly correlated with an increase in oxidative
294 phosphorylation and a decrease in fatty acid biosynthesis in M145.

295 The metabolic switch was shown to be correlated with an enhanced degradation of
296 branched-chain amino acids (valine, leucine and isoleucine), an increase in oxidative
297 phosphorylation and a decrease in fatty acid biosynthesis (**Figure 2D and S4**). An active
298 oxidative phosphorylation relies on an active TCA cycle that generates reduced co-factors
299 whose re-oxidation by the respiratory chain generates a proton gradient that drives ATP
300 synthesis by the ATP synthase. The feeding of the TCA cycle requires acetyl-CoA, as well as
301 nitrogen. Nitrogen likely originates from degradation of glutamate and branched-chain
302 amino acids, whereas acetyl-CoA likely originates from glycolysis, as well as from the
303 degradation of these amino acids as previously demonstrated (Stirrett, Denoya, and
304 Westpheling 2009). Indeed, the model predicts an increased flux through citrate synthase
305 feeding acetyl-CoA into the TCA cycle (**Figure S5A).** The predicted increase in oxidative
306 phosphorylation is supported by the RNA-seq data showing upregulation of enzymes
307 belonging to the respiratory chain (**Figure S5B**). This is consistent with the clear correlation
308 previously reported between high ATP/ADP ratio, resulting from an active oxidative
309 phosphorylation, and actinorhodin production (Esnault et al. 2017). Furthermore, the
310 consumption of acetyl-CoA by the TCA cycle to support the oxidative metabolism logically
311 impairs fatty acids biosynthesis (Esnault et al. 2017).

312

313 The pentose phosphate pathway provides the main redox cofactor NADPH for polyketide
314 biosynthesis, as well as to combat oxidative stress, and its model-predicted flux increase
315 upon initiation of polyketide synthesis (**Figure 2D**) is in agreement with previous studies

316 (Borodina et al. 2008; Jonsbu, Christensen, and Nielsen 2001). A clear positive correlation
317 was also noticed between the biosynthesis of alanine, aspartate and glutamate, which are
318 precursors for CDA and/or coelimycin P1 (**Figure 2D**) and the biosynthesis of these
319 antibiotics. Similar observations were made in the antibiotic-producing *Amycolatopsis sp.*
320 (Gallo et al. 2010). Our EcSco-GEM model proved to be in good agreement with previously
321 reported findings, indicating that it is able to capture *S. coelicolor* metabolic behaviour.

322 Model-assisted characterization of engineered *S. coelicolor* M1152 and its responses to
323 phosphate depletion.

324 As detailed above, EcSco-GEM shed a new light on the metabolic switch in secondary
325 metabolite producing strain M145. *S. coelicolor* M1152 (Gomez-Escribano and Bibb 2011) is
326 a M145 derivative devoid of the four major BGCs and bearing a point mutation in the *rpoB*
327 gene. A better systemic understanding of M1152 metabolism would benefit to its further
328 development as a performing host. To do so, a comparative analysis of gene expression
329 levels and metabolic fluxes was carried out in the strains M145 and M1152.

330 Batch cultivations of M1152 were performed using identical conditions and comparable
331 sampling regimes as for M145 reported above. This enabled a direct comparison of the two
332 strains at a systems level, revealing both expected and unexpected effects of the strains'
333 genetic differences (**Figure 3**). As anticipated, the products of the Cpk, CDA, Red, and Act
334 biosynthetic pathways were undetectable in M1152 (**Figure 3A**). As previously observed
335 (Gomez-Escribano and Bibb 2011), the growth rate of M1152 is reduced compared to M145
336 (0.15 h^{-1} vs 0.21 h^{-1} in the initial exponential growth phase), delaying phosphate depletion
337 by M1152 to 47 hours after inoculation (**Figure 3B**), 12 hours after M145 **(Figure 2B)**.

338 The sampling time points for proteome and transcriptome were adjusted accordingly (**Figure**
339 **3B**), enabling pairwise comparison of measurements between the two strains. Genes
340 responsive to phosphate depletion, members of the PhoP regulon (Nieselt et al. 2010), were
341 used to align the different sample datasets for M145 or M1152 (**Figure 3C**). Principle
342 component analysis of the proteome data confirms high consistency between corresponding
343 biological replicates and incremental changes between sample points for both M145 and
344 M1152 (mainly explained by PC1: 18.6% variance, **Figure 3D**). A clear strain dependent
345 clustering of the data (PC2: 15.5% variance) indicates global significant differences at the
346 protein level. EcSco-GEM was subsequently used to predict metabolic changes in M1152,
347 and interestingly we find that most patterns in M145 are retained in M1152 (**Figure 3E**):
348 fatty acid and nucleotide biosynthesis are still downregulated after phosphate depletion,
349 and similar trends of upregulation at later time points are observed for oxidative
350 phosphorylation, glycine, serine and threonine, and pyruvate metabolism. It is striking that
351 the upregulation of the branched-chain amino acid degradation and the alanine, aspartate,
352 and glutamate metabolism seen as a response to phosphate depletion in M145 is absent in
353 M1152.

354 The different glutamate and glucose consumption rates of M145 and M1152 (**Figure 4A and**
355 **4B**) resulted in substantial metabolic differences between the two strains prior to phosphate
356 depletion. During cultivation on SSBM-P medium, where glutamate is the sole nitrogen
357 source, glucose and glutamate are co-consumed. M1152, as M1146 (Esnault et al. 2017), has
358 an increased growth yield on glucose compared to M145 (**Figure S6**). It thus obtains a larger
359 share of its carbon from glutamate (**Figure 4A and 4B**) and has consequently also a higher
360 nitrogen availability than M145. The increased nitrogen availability does however not
361 increase the secretion of ammonium, indicating that the consumed nitrogen is directed

362 towards growth or production of secondary metabolites. A reduced flux through glycolysis
363 has also been reported previously for strain M1146 (Coze et al. 2013). This might be an
364 effect of the predicted increased concentration of ATP in M1146 compared to M145, which
365 inhibits glucose uptake and phosphofructokinase (Coze et al. 2013; Esnault et al. 2017). Since
366 Act was proposed to act as an electron acceptor reducing the efficiency of the oxidative
367 phosphorylation, it is suggested that the lack of Act in M1146 causes the elevated ATP levels
368 (Esnault et al. 2017). However, we find the largest difference in glycolytic flux at early time
369 points, prior to phosphate depletion and Act production in M145, proving that Act itself
370 cannot explain this observation.

371 The EcSco-GEM predicts the consequences of the reduced glucose uptake of M1152 on its
372 central carbon metabolism, as displayed by mapping relative reaction fluxes from the second
373 sampling time point onto a map of the central carbon metabolism in *Streptomyces* (**Figure**
374 **4C**). The map is based on the reaction network in Sco-GEM and created using Escher (King et
375 al. 2015). A less active glycolysis in M1152 than in M145 leads to a lower carbon flow
376 towards acetyl-CoA and thus lower excretion of acetate compared to M145 (**Figure 4B**).
377 Furthermore, EcSco-GEM reveals an increased flux from glutamate to alpha-ketoglutarate.
378 Indeed, a fraction of the pool of oxaloacetate might be converted into alpha-ketoglutarate
379 by aspartate transaminase to feed the TCA cycle. The rest might be converted into
380 phosphoenolpyruvate (PEP) by PEP carboxykinase for gluconeogenesis because PEP
381 carboxykinase was shown to carry higher fluxes in M1152 than in M145 (**Figure 4C**).

382 Since recent studies have demonstrated a negative correlation and a competition for
383 common precursors between secondary metabolite and triacylglycerol (TAG) biosynthesis in
384 *S. lividans* and *S. coelicolor* (Esnault et al. 2017; Millan-Oropeza et al. 2017; Craney et al.

385 2012), one can speculate that the acetyl-CoA/malonyl-CoA units yielded by glycolysis for the
386 biosynthesis of antibiotics in M145 are being used for enhanced growth and/or fatty acids
387 and TAG biosynthesis in M1152. However, this is likely not the case, as M1152 has rather a
388 reduced growth rate compared to M145, and fatty acid biosynthesis remains downregulated
389 after the switch (**Figure 5**). Malonyl-CoA is predominantly shuttled towards fatty acid
390 biosynthesis through malonyl-CoA-ACP transacylase, and this consumption seems to be well-
391 balanced by the amount of malonyl-CoA produced by acetyl-CoA carboxylase. It is
392 noteworthy that the flux toward this acetyl-CoA/malonyl-CoA drain is 3- to 6-fold larger than
393 the total flux going into secondary metabolite biosynthesis, even after the metabolic switch.
394 We thus propose that together with enhanced nitrogen availability, acetyl-CoA made
395 available from the deletion of these BGCs is used to feed the TCA cycle to support the
396 oxidative metabolism in M1152. This would generate oxidative stress whose toxic effects
397 might be responsible for the growth delay of this strain.

398

399 ## Transcriptome analysis reveal differential expression of global regulators

400 While the proteome data are an integral part of the EcSco-GEM models, RNA-seq data were
401 used to both verify the trends and to gain further insights in the regulatory changes that are
402 not captured by the metabolic models. As the proteomic data, the RNA-seq data showed
403 large global differences between M1152 and M145, revealing 499 differentially expressed
404 genes with a significance threshold of $p<0.01$.

405 Unsupervised clustering of the significantly changed genes reveal differences in regulatory
406 systems related to redox regulation, signalling and secondary metabolism. The significantly
407 changed genes were clustered into 7 groups with K-means clustering, with clusters 1-3

408 containing genes that are upregulated in M1152 compared to M145 and clusters 4-7 vice
409 versa (**Figure S7A and Data Set S1, Tab 5**). A Gene Ontology (Ashburner et al. 2000;
410 The Gene Ontology Consortium 2019) enrichment analysis of the seven clusters was
411 conducted to identify upregulated processes in each of the two strains (**Figure S8**, **cf. Figure**
412 **S7A**).

413 The enriched processes upregulated in M1152 point to increased oxidative stress (**Figure S8**):
414 antioxidant and peroxidase activity (SCO2633 [sodF]; SCO4834-35) in addition to
415 biosynthesis of carotenoid (SCO0185–SCO0188), a known antioxidant (Stahl and Sies 2003;
416 Latifi, Ruiz, and Zhang 2009). The putative proteins within the cytochrome-P450 family
417 (SCO7416–SCO7422) found in cluster 1 might also be linked to increased oxidative stress
418 (Zangar, Davydov, and Verma 2004), but also to oxidation of precursors used for the
419 synthesis of macrolides (Lamb et al. 2003). Indeed, by comparing the time series expression
420 levels for genes related to oxidative stress we observe that the majority of genes related to
421 oxidative stress are upregulated in M1152 (**Figure 6**). These changes correlate to a more
422 active oxidative metabolism, TCA cycle and oxidative stress as predicted by Ec-ScoGEM
423 (**Figure 4**).

424 In cluster 2 we find *scbA* (SCO6266) and its downstream gene *scbC* (SCO6267), which stands
425 out by being almost 6-fold upregulated in M1152. This high expression level is likely due to
426 the deletion of *scbR2* (SCO6286), the last gene selected to be part of the *cpk* BGC (Bednarz,
427 Kotowska, and Pawlik 2019). Besides regulation of the *cpk* cluster, ScbR2 binds upstream of
428 several global regulators of development and secondary metabolism, including AfsK, SigR,
429 NagE2, AtrA, AdpA and ArgR (X. Li et al. 2015). It also acts together with ScbR to regulate
430 ScbA, which produces the y-butyrolactone SCB1. However, when looking at the genes

431 regulated by ScbR (X. Li et al. 2015), we only observe a clear difference in expression for
432 genes regulated by AfsR (phosphorylated by AfsK) (Lee, Umeyama, and Horinouchi 2002;
433 Horinouchi 2003), while this is not the case for genes regulated by ArgR, AdpA or ScbR itself
434 (**Figure S5C-F**).

435 Amongst the genes upregulated in M145, in cluster 4 we find genes related to the redox
436 regulated transcription factor SoxR (Naseer, Shapiro, and Chander 2014), and a similar
437 pattern is observed for the entire SoxR regulon (**Figure S7B**). SoxR is known to react directly
438 to the presence of actinorhodin (Dela Cruz et al. 2010; Shin et al. 2011), and indeed, in M145
439 this group of genes follows the production profile of actinorhodin, while their expression
440 remains low in M1152 since Act is not produced. The benzoquinone Act, as electron
441 acceptor, is thought to reduce respiration efficiency and thus energy charge as well as to
442 combat oxidative stress (Esnault et al. 2017). Consistently, the RNA-seq data revealed that
443 the ATP-synthase gene cluster (SCO5366–SCO5374) was upregulated almost 2-fold in M1152
444 compared to M145, most prominently in the stationary phase during Act production (**Figure**
445 **S7C**). This agrees with observations in the M1146 strain (Coze et al. 2013). Cluster 4 also
446 contains the genes directly up- and downstream of the deleted actinorhodin BGC in M1152
447 (SCO5071–SCO5072, encoding 3-hydroxyacyl-CoA dehydrogenase, and SCO5091–SCO5092,
448 encoding a two-component flavin-dependent monooxygenase system) (Valton et al. 2008).
449 In clusters 5, 6 and 7 we find genes with reduced expression in M1152, and the enriched
450 processes are related to cellular and iron ion homeostasis, development, signalling and
451 morphology. This corresponds to the delayed sporulation observed for M1152 (Gomez-
452 Escribano and Bibb 2011).

453

454 ## Elevated expression of ribosomal proteins in M1152 after phosphate depletion

455 An increased transcription of genes encoding ribosomal proteins could be observed in
456 M1152 after phosphate depletion (**Figure S7D**). The *rpoB* mutation of the RNA polymerase
457 present in M1152 is thought to induce a conformational change mimicking the binding of
458 guanosine tetraphosphate (ppGpp) to this enzyme (Hu, Zhang, and Ochi 2002). ppGpp is
459 synthesized in response to nutritional stress and reduces the transcription of genes related
460 to active growth, such as genes encoding ribosomal RNAs and ribosomal proteins (Burgos et
461 al. 2017), whereas it upregulates those involved in development/differentiation and
462 antibiotic production (Hesketh et al. 2007; Srivatsan and Wang 2008). In consequence the
463 upregulation of ribosomal proteins was unexpected in M1152, especially since the
464 expression of the ppGpp regulon was not found to be significantly changed in M1152 (**Figure**
465 **S5G and S5H**). We hypothesize that the ribosomal upregulation originates from the higher
466 ATP content of M1152 compared to M145 post phosphate depletion, as high nucleoside
467 triphosphate levels are known to have a positive impact on ribosome synthesis (Gaal et al.
468 1997). Such difference in ribosomal protein expression is mainly seen in the antibiotic
469 production phase and correlated with production of Act in M145, which has a negative
470 impact on the energetic state of the cell (Esnault et al. 2017).

471 ## Reduced production of the polyketide germicidin in M1152

472 One could reasonably anticipate that the production of a secondary metabolite would
473 increase if other drains competing for same precursor compounds were removed from the
474 organism by gene deletion. However, the production rate of the polyketides germicidin A
475 and B (Chemler et al. 2012), autologous to both M145 and M1152, were reduced in M1152
476 by 92% and 82% for germicidin A and B, respectively (**Figure 7**). This could be explained by
477 the more active oxidative metabolism of M1152 compared to M145, as suggested by the

478 enzyme-constrained model (**Figure 4**) and supported by the upregulation of genes
479 associated with oxidative stress (**Figure 6**). In M1152 the pool of acetyl-CoA rather feeds the
480 TCA cycle instead of being directed towards germicidin biosynthesis.

481 To further elucidate the cause of the reduced production in M1152, we also measured
482 germicidin production in the intermediate strain M1146 (**Figure 7, Figure S7E**), which does
483 not feature the *rpoB* mutation but is missing the 4 BGCs also deleted in M1152 (Gomez-
484 Escribano and Bibb 2011). The production rate of germicidin A and B in M1146 was found to
485 be reduced by 27% and 25%, respectively, compared to M145. In comparison to the strong
486 reduction in germicidin production that can be assigned to the *rpoB* mutation in M1152,
487 removal of only the 4 BGCs in M1146 has a moderate effect on germicidin production. This
488 conforms with the minor contribution of the BGCs compared to fatty acid biosynthesis on
489 the total consumption of malonyl-CoA (**Figure 5**). Nonetheless, it remains contradictory that
490 the removal of polyketide precursor drains negatively impacts the production of other
491 polyketides.

492 Discussion

493 In this work, we carried out a multi-omics study to compare the metabolic changes of
494 *Streptomyces coelicolor* M145 and the BGC-deletion mutant M1152 during batch
495 fermentation. The defined cultivation medium used in this work was chosen because it
496 supports sufficient growth and a delayed, well-defined onset of secondary metabolism,
497 necessary to study the metabolic switch (Wentzel, Bruheim, et al. 2012). We aimed at
498 defining the metabolic features differing between the two strains, both during exponential
499 growth and stationary phase after phosphate depletion.

500 To achieve this from a systems biology perspective, we combined time-course sampled
501 cultivation and transcriptome analysis with enzyme-constrained genome-scale models
502 generated with proteome data. Such genome-scale models are extensively used to connect
503 transcriptome- and proteome data to metabolic fluxes. Leveraging metabolic simulations to
504 contextualize transcriptional changes is mainly impacted by the quality of the computational
505 model used. Here, two teams joined efforts to improve a consensus model of *S. coelicolor*,
506 yielding a comprehensive model useful for the scientific community.

507 Genome-scale models provide hypothesis for slow growth of M1152

508 The reduced growth rate of M1152 is correlated with reduced glucose uptake and enhanced
509 glutamate uptake compared to M145. This is expected to lead to a less active glycolysis but a
510 more active TCA cycle, and thus, a more active oxidative metabolism in M1152 compared to
511 M145. An active oxidative metabolism is known to generate oxidative stress, and indeed, the
512 *in vivo* data, as well as the genome-scale model, predict an increased oxidative stress in
513 M1152. The toxicity of oxidative stress might, at least in part, be responsible for the growth
514 delay of M1152, while the *rpoB* mutation may add to this phenotype, since one of the
515 functions of the ppGpp-associated RNA polymerase is to promote a growth arrest in
516 conditions of nutritional stress.

517 Further development may improve M1152 as host for heterologous expression

518 The strain M1152 has several advantages as a host for heterologous production of secondary
519 metabolites. The deletion of the 4 major BGCs not only removes presumed competing drains
520 for valuable precursors, but also generates a clean background to ease the identification of
521 novel products by mass spectrometry. M1152 was already proven to be more efficient than
522 M145 and M1146 in heterologous production of the nitrogen-containing antibiotics

523 chloramphenicol and congocidine, as well as Act production from reintroduction of its BGC
524 (Gomez-Escribano and Bibb 2011). Strains M1146 and M1152 produce, respectively, 3- to 5-,
525 and 20- to 40-fold more chloramphenicol and congocidine from respective heterologous
526 clusters than M145, a clear demonstration of the huge impact on production due to the *rpoB*
527 mutation. While this contrasts with our data showing that M1152 has the lowest production
528 of germicidin, it is relevant to note that chloramphenicol and congocidine are non-ribosomal
529 peptide synthases relying on amino acids rather than malonyl-CoA as precursors. Although
530 our data shows reduced degradation of branched-chain amino acids and metabolism of
531 alanine, asparate and glutamate as the clearest metabolic divergence upon phosphate
532 depletion in M1152, since congocidine and chloramphenicol are based on aromatic amino
533 acids the connection to increased production of these NRPs is not obvious. Another option is
534 that the increased oxidative metabolism in M1152 provides more redox cofactors to drive
535 the synthesis of these molecules. If competition for valuable precursors was rate-limiting,
536 the absence of the polyketides actinorhodin and coelimycin P1 should at least enhance the
537 production of germicidin, all being dependent on malonyl-CoA. Moreover, differences in
538 cultivation media further convolute cross-study comparisons: the aforementioned study use
539 a complex growth medium while we used a defined medium with glucose and glutamate,
540 which has previously been optimized for studying the metabolic switch (Wentzel, Bruheim,
541 et al. 2012).

542 Furthermore, (re-)introduction of a (secondary) copy of germicidin synthase gene *gcs* in
543 strains M1152 and M1317—derived from M1152 by additional removal of three Type III PKS
544 genes including *gcs*—gave a 7.8 and 10.7-fold increase in germicidin production,
545 respectively, compared to M1152 with only the native copy of *gcs* (Thanapipatsiri et al.
546 2015). Thus, the largest increase in production is not achieved by removal of competing

547 precursor drains, but rather effected by the re-introduction of *gcs*, probably because
548 expression of the inserted gene is not constrained by the same regulatory mechanism as the
549 native gene.

550

551 Although earlier work has suggested a competition for common precursors between fatty
552 acids and secondary metabolites biosynthesis (Craney et al. 2012), our results suggest that
553 other approaches than deletion of competing precursor drains may be more efficient in the
554 development of an optimized expression host, and it seems likely that different classes of
555 BGCs may require different hosts for maximal production. Our comparative analysis of M145
556 and M1152 supports this development, not only as a systemic description connecting non-
557 trivial associations between phenotypic, genetic and metabolic differences, but also by
558 highlighting cellular processes that seems to be out of balance in M1152. These includes
559 upregulation of ribosomal genes, most likely an effect of the *rpoB* mutation, and increased
560 oxidative metabolism and oxidative stress. Since Act itself works as an electron acceptor one
561 may hypothesize that its presence could relieve some of this stress. Another approach is to
562 reintroduce *scbR2* to avoid influencing the related regulators of development and secondary
563 metabolism.

564 Although *S. coelicolor* seems to have a complex and not fully elucidated regulatory system
565 several studies have shown that manipulation of regulatory genes can affect production of
566 secondary metabolites (Jones et al. 2011; D.-J. Kim et al. 2003; Okamoto et al. 2003;
567 Rodriguez et al. 2012). The complex regulation of secondary metabolite biosynthesis makes
568 rational strain design difficult (Liu et al. 2013), but black-box approaches including random
569 mutations and screening are still viable approaches for strain development (van den Berg et

570 al. 2008; Crook and Alper 2012). The Sco-GEM can aid this development by predicting the
571 impact of these genetic alterations and to interpret 'omics data.

572 Limitations of the Study

573 We have performed a thorough comparison, of *S. coelicolor* M1145 and M1152, but to fully
574 attribute changes in metabolism to the different genetic modifications as well as to unravel
575 possible epistatic interactions we believe that a comprehensive analysis that also include the
576 intermediate strain M1146, and possibly also an M145 strain featuring only the *rpoB*
577 mutation (Xu et al. 2002), will be necessary.

578 Resource availability

579 Lead Contact

580 Further information and requests for resources and reagents should be directed to and will
581 be fulfilled by the Lead Contact, Eduard J Kerkhoven (eduardk@chalmers.se).

582 Materials Availability

583 This study did not generate new unique reagents.

584

585 Data and Code Availability

586 The models and scripts generated during this study are available at GitHub
587 (https://github.com/SysBioChalmers/Sco-GEM). Here, the latest version of the Sco-GEM is
588 available in both YAML and SBML level 3 Version 1. Additionally, users can contribute to
589 further model development by posting issues or suggest changes. The proteomics data have
590 been deposited to the ProteomeXchange Consortium via the PRIDE (Perez-Riverol et al.

591 2019) partner repository with the dataset identifier PXD013178. Normalized proteome data
592 is also available in **Data Set S1, Tab 14.** The transcriptomics data have been deposited in
593 NCBI's Gene Expression Omnibus and are accessible under accession number GSE132487
594 (M145) and GSE132488 (M1152). Normalized counts are also found in **Data Set S1, Tab 15.**

595

596 Acknowledgements

597 The authors would like to acknowledge Bogdan I. Florea of Leiden University, Leiden,
598 Netherlands, for running and monitoring the proteome measurements, and the bio-organic
599 synthesis group at Leiden University for providing the opportunity to use their
600 instrumentation. The authors would also like to acknowledge co-workers at SINTEF Industry,
601 Trondheim, Norway: Ingemar Nærdal, Anna Lewin and Kari Hjelen for running the batch
602 fermentations and Anna Nordborg, Janne Beate Øiaas and Tone Haugen for performing
603 offline analyses and the germicidin analytics. The RNA-Seq sequencing was carried out by
604 c.ATG, Tübingen, Germany.

605 This study was conducted in the frame of ERA-net for Applied Systems Biology (ERA-SysAPP)
606 project SYSTERACT and the project INBioPharm of the Centre for Digital Live Norway
607 (Research Council of Norway grant no. 248885), with additional support of SINTEF internal
608 funding.

609 Author contributions

610 Conceptualization, E.K., E.A., A.W., S.S., A.S.Y. and T.K. Methodology and software, E.K., S.S.,
611 A.S.Y. and T.K. Validation and formal analysis, C.D., K.N., D.V.D., S.S., T.K., E.K. Investigation,
612 T.K., A.W., S.S., E.K. Data curation, S.S., T.K. Writing - original draft, S.S., T.K., D.V.D., C.D.,

613 K.N. Writing – review & editing, all authors. Visualization, S.S., E.K., C.D., D.V.D. Supervision,

614 A.W., E.A., E.K., G.W. Project administration, A.W. Funding acquisition: A.W., E.K., E.A., G.W.

615 Declaration of Interests

616 The authors declare no competing interests.

617

618 Figures

619 **Figure 1: Sco-GEM development and analysis.** A) Schematic overview of the various steps in

620 the Sco-GEM reconstruction process. B) The overall memote score and number of genes,

621 reactions and metabolites for the 7 published *S. coelicolor* GEMs. C) Assessment of the model

622 quality by comparing *in vivo* observations with *in silico* predictions across in total 241 tests:

623 accuracy = 0.80; sensitivity = 0.96; specificity = 0.48; Matthews Correlation Coefficient = 0.53.

624 D) The change in Gibbs free energy for 770 reactions that were annotated as either reversible

625 or forward (i.e. forward irreversible) in the model prior curation of reaction reversibility. The

626 histogram is truncated at -105 kJ/mol, and more negative values are assigned to the leftmost

627 bin. E) Analysis and comparison of the directionality and reversibility of reactions prior

628 curation and the direction inferred from the change in Gibbs free energy as estimated by

629 eQuilibrator. Reactions labelled "forward" or "backward" are irreversible. F) Overview of the

630 369 transport reactions included in Sco-GEM, whereof 42 were curated and 65 added during

631 this work. The inner ring categorizes the reactions into 9 different subgroups, while the outer

632 ring displays the amount of curated and added reactions within each category. In the outer

633 ring, the sections representing curated and new reactions are hatched and dotted,

634 respectively. G) Comparison of cumulative flux variability distributions in Sco-GEM and EcSco-
635 GEM.

636

637 **Figure 2: Batch cultivation of *S. coelicolor* M145 and the effect of phosphate depletion.**
638 Compounds produced (A) and consumed (B) during batch fermentation of *S. coelicolor* M145.
639 Time points for sampling for transcriptome and proteome analysis are indicated with red
640 triangles. The dashed vertical line indicates when phosphate in the medium has been
641 depleted. Error bars are standard deviations of three biological replicates. CDW, Cell Dry
642 Weight; Red, undecylprodigiosin; TBP, Total Blue Pigments/actinorhodins; CO_2 volume
643 corrected respiration; D-Glc, D-glucose; L-Glu, L-glutamate; PO_4, phosphate. C) Comparison of
644 previously published microarray data (Nieselt et al. 2010) and RNA-seq data (this study) for
645 genes previously found to respond to phosphate depletion (Nieselt et al. 2010). The
646 transparent lines correspond to individual genes, while the bold lines represent the average
647 expression level for each data set. D) Clustered heatmap of CO_2-normalized Z-scores for each
648 of the top 10 varying pathways plus the pathways for the 4 major BGCs in M145, as revealed
649 by simulations with the proteomics-integrated EcSco-GEM model. The pathways are sorted
650 based on hierarchical clustering to facilitate visual interpretation of similarity between
651 pathways. The dashed vertical line indicates the time point of the metabolic switch. E) RNA-
652 seq data of the 4 major BGCs show the onset of biosynthesis of actinorhodin (Act), calcium-
653 dependent antibiotic (CDA), coelimycin P1 (Cpk) and undecylprodigiosin (Red) at different
654 time points during the batch fermentations of M145.

655

656 **Figure 3: Batch cultivation of *S. coelicolor* M1152.** Compounds produced (A) and consumed
657 (B) during batch fermentation of *S. coelicolor* M1152. Time points for sampling for
658 transcriptome and proteome analysis are indicated with red triangles. The dashed vertical line
659 indicates when phosphate in the medium has been depleted. Error bars are standard
660 deviations of three biological replicates. CDW, Cell Dry Weight; Red, undecylprodigiosin; TBP,
661 Total Blue Pigments/actinorhodins; CO_2, volume corrected respiration; D-Glc, D-glucose; L-
662 Glu, L-glutamate; PO_4, phosphate. C) Alignment of sample time points of M145 and M1152
663 cultivations based on the expression profiles of genes that were earlier found to respond to
664 phosphate depletion in respect to the metabolic switch (Nieselt et al. 2010). D) Principle
665 component analysis of the proteomics data for M145 (triangles) and M1152 (circles), for each
666 time-point and culture. The first principal component separates the time points while the
667 second principal component separates the two strains. E) CO_2-normalized Z-scores of pathway
668 fluxes predicted by EcSco-GEM for 10 of the most varying pathways in M145 and M1152. To
669 make this heatmap comparable to the results for M145 (**Figure 2D**), the data is standardized
670 for both strains simultaneously and the row order is identical.

671

672 **Figure 4: Predicted carbon fluxes in M145 and M1152.** A) The ratio between estimated uptake
673 rates of glucose and glutamate for each sample time point for M145 and M145 shows that
674 M1152 acquires a smaller part of its carbon from glucose compared to M145. B) Bar chart
675 showing CO2-normalized fluxes for the second sampling time point for M145 and M1152, i.e.
676 after 29 and 41 hours, respectively. There is a clear difference in the uptake of glucose and
677 production of acetate, while the rates are comparable for the consumption of glutamate and
678 secretion of Ammonium. C) Comparison of predicted fluxes for the second sampling time

679 points shows clear differences between the two strains in their relative utilization of the
680 glycolysis and TCA cycle. The strength of the colour of the lines correspond to the flux
681 difference between the strains; green reactions have higher flux in M1152, and red reactions
682 have higher flux in M145.

683

684 **Figure 5: Production and consumption of malonyl-CoA as the branching point between fatty**
685 **acid biosynthesis and production of polyketides**. Both panels display CO2-normalized fluxes
686 for both M145 and M1152 for all sampling time points as predicted by EcSco-GEM. The left
687 panel shows the sources of malonyl-CoA, namely acetyl-CoA carboxylase (ACCOAT; blue) and
688 acetyl-CoA carboxytransferase (ACCOAT_1; orange). We observe a downregulation of the
689 malonyl-CoA production after the metabolic switch (between time point 3 and 4) in both
690 strains. The right panel presents reactions consuming malonyl-CoA. The consumption is
691 dominated by malonyl-CoA-ACP transacylase (MCOATA) leading to biosynthesis of fatty acids.
692 The other drains for malonyl-CoA are the pathways encoded by the 4 major BGCs (Act, Cpk,
693 Red and CDA) in addition to biflaviolin synthase (THYDNAPS).

694

695 **Figure 6: Heatmap displaying log-transformed RNA-seq data of genes associated with**
696 **oxidative stress.** The genes included are related to oxidative stress and either present in Sco-
697 GEM or within the 499 differentially expressed genes. These genes are categorized based on
698 their functional annotation to distinguish differences and similarities between these
699 functional groups. To further enhance visual interpretatioxn the genes are ordered based on
700 hierarchical clustering to align genes with similar expression profiles across M145 and M1152
701 next to each other.

702

703 **Figure 7: Concentrations of germicidin A and B produced by M145, M1146 and M1152.** The
704 concentrations are normalized by the biomass of each strain. The shaded regions display the
705 uncertainty range (± 1 standard deviation) based on three replicate cultivations. Note that the
706 growth rate is different between the strains, displayed by the vertical lines representing
707 phosphate depletion at 35, 38 and 47 hours for M145, M1146 and M1152, respectively.

708 Supplemental Figures

709 **Figure S1: Reaction subsystems and origin.** The number of reactions in Sco-GEM in each of
710 the 15 subsystems, and from which model they originate from. The other reactions (orange)
711 are added during reconstruction of Sco-GEM.

712 **Figure S2: Gene clusters associated with metabolic switch.** RNA-seq (left column) and
713 proteomics (right column) from M145 of the 8 gene clusters associated with the metabolic
714 switch as previously identified (Nieselt et al. 2010). The 8 clusters are: A) genes related to
715 ribosomal proteins; B) genes related to nitrogen metabolism; C) Cpk gene cluster; D) genes
716 related to development; E) genes upregulated in response to phosphate depletion; F) genes
717 involved in synthesis of phosphate-free polymers; G) Act gene cluster; H) Red gene cluster

718 **Figure S3: Log-transformed expression levels of genes related to nitrogen metabolism.** The
719 order of the genes is determined by hierarchical clustering to align genes with similar
720 expression profiles next to each other. From the log2-transformed RNA-seq data we observe
721 that glutamate import (SCO5774-5777), the glutamate sensing system *gluR-gluK* (SCO5778
722 and SCO57779), *glnR* (SCO4159) and *glnA* (SCO2198) are downregulated subsequent to
723 phosphate depletion. The phosphate depletion occurs between the third and fourth time

724 point, i.e. at 35 and 47 hours for M145 and M1152, respectively. We also observe that the first
725 time point in M145 is very different from all other samples.

726

727 **Figure S4: Clustered heatmaps of Z-score based on CO_2-normalized sum of fluxes of all**
728 **pathways standardized within each pathway and separated into different subsystems /**
729 **parts of the metabolism.** A) Central carbon metabolism. B) Amino acid metabolism. C)
730 Metabolism of vitamins and cofactors. D) Pathways of Biosynthetic gene clusters. E) Lipid
731 metabolism. F) Oxidative stress. G) Degradation of toxic compounds. H) All other pathways.
732 For all panels only pathway with a minimum flux of 1e-8 mmol (g DW)$^{-1}$ h^{-1} were included.

733 **Figure S5**: **RNA-seq, proteome and flux prediction of specific gene clusters and reactions.** A)
734 This panel display increasing CO2-normalized flux through citrate synthase (CS) and isocitrate
735 dehydrogenase (ICDHyr) at later time points in M145 as predicted by EcSco-GEM. These two
736 reactions are both part of the TCA cycle, converting acetyl-CoA to citrate (citrate synthase)
737 and isocitrate to alpha-ketogluterate (isocitrate dehydrogenase). B) Log2 normalized
738 expression data of genes involved in oxidative phosphorylation for M145 (blue) and M1152
739 (orange). The average expression level is higher in M1152 than in M145 but increasing at later
740 time points for both strains. The expression profiles are only partially overlapping along the x-
741 axis (hours after inoculation) because of the reduced growth and therefore delayed cultivation
742 of M1152. C-H) Comparison of log2 normalized expression data as calculated with (log2
743 M145)-log2(M1152), where positive values indicate upregulation in M145 relative to M1152,
744 and vice versa for negative values. C) Increased expression of genes of the AfsR regulon in
745 M145, while no significant difference in expression is observed for (D) ScbR regulon; (E) AdpA
746 regulon; (F) ArgR regulon; (G) genes induced by ppGpp; and (H) genes repressed by ppGpp.

747 **Figure S6**: **Biomass yield on glucose and glutamic acid.** M1152 (orange) has a higher growth
748 yield on glucose than M145 (blue). The yield on glutamic acid (dashed line) is similar between
749 the two strains.

750 **Figure S7: Analysis of transcriptome data of genes.** A) The heatmap display the mean
751 standardized log2 expression levels for the 7 clusters of differentially expressed genes as
752 determined by unsupervised clustering (k-means). Cluster 1-3 are upregulated in M1152,
753 while the last four (cluster 4-7) are upregulated from the beginning or at later time points in
754 M145. B-D) Comparison of log2 normalized expression data as calculated with (log2 M145)-
755 log2(M1152), where positive values indicate upregulation in M145 relative to M1152, and vice
756 versa for negative values. B) Genes in the SoxR regulon are reducing expression in M1152 at
757 later time points. C) Almost all genes in the ATP-synthase cluster are up-regulated in M1152
758 after the first time point. D) The transcription of ribosomal protein genes after the metabolic
759 switch is increased in M1152 compared to M145. E) Batch cultivation data of *S. coelicolor*
760 M1146, showing volume corrected respiration (CO_2), phosphate (PO_4) and cell dry weight
761 (CDW). Error bars are standard deviations of three biological replicates.

762 **Figure S8: Gene Ontology enrichment analysis of the 7 clusters identified in the 499**
763 **differentially expressed genes, categorized by function into four clustered heatmaps.**

764 Each heatmap shows the p-value for the enrichment of each GO-process. A) Genes related to
765 reactive oxygen species, the ribosome or development process and cell wall formation. B)
766 Oxireductase and iron / metal ion homeostasis. C) Regulation, biosynthesis and metabolism
767 related to RNA and DNA. D) All other GO-annotations. E) This color palette is the legend for
768 the column colors on top of each heatmap which displays which of the seven clusters each
769 gene belongs to. The red palette covers cluster 1-3 (upregulated in M1152), while the blue

770 palette covers cluster 4-7 (upregulated in M145). Note that no GO-processes were enriched
771 for the genes in cluster 2.

772 **Figure S9: Comparison of normalization methods of randomly sampled fluxes**. Heatmap
773 showing mean flux values normalized by A) total carbon uptake from glucose and glutamate,
774 B) CO_2 production, C) sum of all fluxes and D) growth rate. Because the mean flux values in
775 these reactions are different by several orders of magnitude, we display the data as
776 standardized values (for each reaction).

777

778 Other Supplemental material

779 **Supplemental Information:** The memote report of Sco-GEM and the Transparent Methods
780 are provided in the Supplemental Information.

781

782 **Data Set S1**

783 **Tab 1:** Detailed overview of the script performing the reconstruction of Sco-GEM.

784 **Tab 2:** Comparison of the new biomass reaction in Sco-GEM with the biomass reaction in
785 iAA1259.

786 **Tab 3:** Reversibility prior update, calculated change in Gibbs free energy and standard
787 deviation of the calculated change in Gibbs free energy of 770 reactions in Sco-GEM.

788 **Tab 4:** Overview of all transport reactions added or curated during the process of Sco-GEM
789 model development, and the metabolites added along with the new transport reactions.

790 **Tab 5:** Genes present in the 7 clusters identified with K-Means clustering of the
791 differentially expressed genes.

792 **Tab 6:** Sco4 ID, name and Sco-GEM ID of the reactions added from Sco4 to Sco-GEM.

793 **Tab 7:** Sco4 ID, name and Sco-GEM ID of the metabolites added from Sco4 to Sco-GEM

794 **Tab 8:** Reaction ID, name and gene annotation of reactions added from iAA1259 to Sco-
795 GEM.

796 **Tab 9:** List of reactions modified according to iAA1259.

797 **Tab 10**: Metabolite ID and name of metabolites added from Sco4 to Sco-GEM.

798 **Tab 11**: List of SBO terms used in Sco-GEM

799 **Tab 12**: Single, pair and triplets of reactions which reduced model accuracy, in total 56
800 different reactions. The reversibility of these reactions was not changed according to the
801 predicted change in Gibbs free energy.

802 **Tab 13**: Manual curation of the reversibility of the 82 reactions involving ATP predicted to
803 be reversible by eQuilibrator.

804 **Tab 14**: Normalized proteome data for M145 and M1152. M145 is cultivated in F516-F518,
805 while M1152 is cultivated in F519, F521, F522. Re-index IDs corresponds to the strain,
806 fermentation-number (F516-F522), a unique number describing the experiment, and a
807 numbering of the time points from 1 to 9 (P1-P9). I.e. the Re-indexed ID M145_F516_P2
808 represents the second timepoint of fermentation 516 with the strain M145. In the original
809 IDs (row below) the P-number represents time after inoculation (in hours).

810 **Tab 15**: Normalized RNA-seq data for all six fermenters. M145 is cultivated in F516-F518,
811 while M1152 is cultivated in F519, F521, F522. Re-index IDs corresponds to the strain,
812 fermentation-number (F516-F522), a unique number describing the experiment, and a
813 numbering of the time points from 1 to 9 (P1-P9). I.e. the Re-indexed ID M145_F516_P2
814 represents the second timepoint of fermentation 516 with the strain M145. In the original
815 IDs (row below) the P-number represents time after inoculation (in hours).

816 **Tab 16**: List of genes within each cluster known to be associated with the metabolic switch.

817

818

819 # References

820 Alam, Mohammad T, Maria E Merlo, The STREAM Consortium (stream), David A Hodgson,
821 Elizabeth MH Wellington, Eriko Takano, and Rainer Breitling. 2010. 'Metabolic
822 Modeling and Analysis of the Metabolic Switch in Streptomyces Coelicolor'. *BMC*
823 *Genomics* 11 (1): 202. https://doi.org/10.1186/1471-2164-11-202.

824 Amara, Adam, Eriko Takano, and Rainer Breitling. 2018. 'Development and Validation of an
825 Updated Computational Model of Streptomyces Coelicolor Primary and Secondary
826 Metabolism'. *BMC Genomics* 19 (1): 519. https://doi.org/10.1186/s12864-018-4905-5.

827 Ashburner, M., C. A. Ball, J. A. Blake, D. Botstein, H. Butler, J. M. Cherry, A. P. Davis, et al. 2000.
828 'Gene Ontology: Tool for the Unification of Biology. The Gene Ontology Consortium'.
829 *Nature Genetics* 25 (1): 25–29. https://doi.org/10.1038/75556.

830 Aung, Hnin W., Susan A. Henry, and Larry P. Walker. 2013. 'Revising the Representation of
831 Fatty Acid, Glycerolipid, and Glycerophospholipid Metabolism in the Consensus Model

832 of Yeast Metabolism'. *Industrial Biotechnology* 9 (4): 215–28.
833 https://doi.org/10.1089/ind.2013.0013.
834 Bar-Even, Arren, Avi Flamholz, Elad Noor, and Ron Milo. 2012. 'Thermodynamic Constraints
835 Shape the Structure of Carbon Fixation Pathways'. *Biochimica et Biophysica Acta (BBA)*
836 *- Bioenergetics* 1817 (9): 1646–59. https://doi.org/10.1016/j.bbabio.2012.05.002.
837 Battke, Florian, Stephan Symons, and Kay Nieselt. 2010. 'Mayday--Integrative Analytics for
838 Expression Data'. *BMC Bioinformatics* 11 (March): 121. https://doi.org/10.1186/1471-
839 2105-11-121.
840 Bednarz, Bartosz, Magdalena Kotowska, and Krzysztof J. Pawlik. 2019. 'Multi-Level Regulation
841 of Coelimycin Synthesis in Streptomyces Coelicolor A3(2)'. *Applied Microbiology and*
842 *Biotechnology* 103 (16): 6423–34. https://doi.org/10.1007/s00253-019-09975-w.
843 Bentley, Sd D., Kf F. Chater, A.-M. A-M Cerdeño-Tárraga, G. L. Challis, N. R. Thomson, K. D.
844 James, D. E. Harris, et al. 2002. 'Complete Genome Sequence of the Model
845 Actinomycete Streptomyces Coelicolor A3(2).' *Nature* 417 (6885): 141–47.
846 https://doi.org/10.1038/417141a.
847 Berg, Marco A. van den, Richard Albang, Kaj Albermann, Jonathan H. Badger, Jean-Marc Daran,
848 Arnold J. M. Driessen, Carlos Garcia-Estrada, et al. 2008. 'Genome Sequencing and
849 Analysis of the Filamentous Fungus *Penicillium Chrysogenum*'. *Nature Biotechnology*
850 26 (10): 1161–68. https://doi.org/10.1038/nbt.1498.
851 Bordel, Sergio, Rasmus Agren, and Jens Nielsen. 2010. 'Sampling the Solution Space in
852 Genome-Scale Metabolic Networks Reveals Transcriptional Regulation in Key
853 Enzymes'. *PLOS Computational Biology* 6 (7): e1000859.
854 https://doi.org/10.1371/journal.pcbi.1000859.

855 Borodina, Irina, Preben Krabben, and Jens Nielsen. 2005. 'Genome-Scale Analysis of
856 Streptomyces Coelicolor A3(2) Metabolism.' *Genome Research* 15 (6): 820–29.
857 https://doi.org/10.1101/gr.3364705.
858 Borodina, Irina, Jeroen Siebring, Jie Zhang, Colin P. Smith, Geertje van Keulen, Lubbert
859 Dijkhuizen, and Jens Nielsen. 2008. 'Antibiotic Overproduction in Streptomyces
860 Coelicolor A3(2) Mediated by Phosphofructokinase Deletion'. *Journal of Biological*
861 *Chemistry* 283 (37): 25186–99. https://doi.org/10.1074/jbc.M803105200.
862 Braesel, Jana, Tuan Anh Tran, and Alessandra S. Eustáquio. 2019. 'Heterologous Expression of
863 the Diazaquinomycin Biosynthetic Gene Cluster'. *Journal of Industrial Microbiology &*
864 *Biotechnology*, May. https://doi.org/10.1007/s10295-019-02187-1.
865 Burgos, Hector L., Kevin O'Connor, Patricia Sanchez-Vazquez, and Richard L. Gourse. 2017.
866 'Roles of Transcriptional and Translational Control Mechanisms in Regulation of
867 Ribosomal Protein Synthesis in Escherichia Coli'. *Journal of Bacteriology* 199 (21).
868 https://doi.org/10.1128/JB.00407-17.
869 Bystrykh, L. V., M. A. Fernández-Moreno, J. K. Herrema, F. Malpartida, D. A. Hopwood, and L.
870 Dijkhuizen. 1996. 'Production of Actinorhodin-Related "Blue Pigments" by
871 Streptomyces Coelicolor A3(2)'. *Journal of Bacteriology* 178 (8): 2238–44.
872 Castro, Jean Franco, Valeria Razmilic, Juan Pablo Gomez-Escribano, Barbara Andrews, Juan A.
873 Asenjo, and Mervyn J. Bibb. 2015. 'Identification and Heterologous Expression of the
874 Chaxamycin Biosynthesis Gene Cluster from Streptomyces Leeuwenhoekii'. *Appl.*
875 *Environ. Microbiol.* 81 (17): 5820–31. https://doi.org/10.1128/AEM.01039-15.
876 Chakrabarty, A. M. 1998. 'Nucleoside Diphosphate Kinase: Role in Bacterial Growth, Virulence,
877 Cell Signalling and Polysaccharide Synthesis'. *Molecular Microbiology* 28 (5): 875–82.
878 https://doi.org/10.1046/j.1365-2958.1998.00846.x.

879 Chandra, Govind, and Keith F. Chater. 2014. 'Developmental Biology of Streptomyces from the
880 Perspective of 100 Actinobacterial Genome Sequences'. *FEMS Microbiology Reviews*
881 38 (3): 345–79. https://doi.org/10.1111/1574-6976.12047.
882 Chemler, Joseph A., Tonia J. Buchholz, Todd W. Geders, David L. Akey, Christopher M. Rath,
883 George E. Chlipala, Janet L. Smith, and David H. Sherman. 2012. 'Biochemical and
884 Structural Characterization of Germicidin Synthase: Analysis of a Type III Polyketide
885 Synthase That Employs Acyl-ACP as a Starter Unit Donor'. *Journal of the American*
886 *Chemical Society* 134 (17): 7359–66. https://doi.org/10.1021/ja2112228.
887 Coze, Fabien, Françoise Gilard, Guillaume Tcherkez, Marie-Joëlle Virolle, and Armel
888 Guyonvarch. 2013. 'Carbon-Flux Distribution within Streptomyces Coelicolor
889 Metabolism: A Comparison between the Actinorhodin-Producing Strain M145 and Its
890 Non-Producing Derivative M1146'. *PLOS ONE* 8 (12): e84151.
891 https://doi.org/10.1371/journal.pone.0084151.
892 Craney, Arryn, Cory Ozimok, Sheila Marie Pimentel-Elardo, Alfredo Capretta, and Justin R.
893 Nodwell. 2012. 'Chemical Perturbation of Secondary Metabolism Demonstrates
894 Important Links to Primary Metabolism'. *Chemistry & Biology* 19 (8): 1020–27.
895 https://doi.org/10.1016/j.chembiol.2012.06.013.
896 Crook, N, and HS Alper. 2012. 'Classical Strain Improvement. Engineering Complex Phenotypes
897 in Industrial Strains'. *John Wiley & Sons, Inc.). Http://Dx. Doi.*
898 *Org/10.1002/9781118433034. Ch1 Daniell, J., Nagaraju, S., Burton, F., Köpke, M., and*
899 *Simpson, SD (2016). Low-Carbon Fuel and Chemical Production by Anaerobic Gas*
900 *Fermentation. Adv. Biochem. Eng. Biotechnol* 156: 293–321.
901 Dela Cruz, Rica, Yang Gao, Sahitya Penumetcha, Rebecca Sheplock, Katherine Weng, and
902 Monica Chander. 2010. 'Expression of the Streptomyces Coelicolor SoxR Regulon Is

903 Intimately Linked with Actinorhodin Production'. *Journal of Bacteriology* 192 (24):
904 6428–38. https://doi.org/10.1128/JB.00916-10.
905 Dobson, Paul D, Kieran Smallbone, Daniel Jameson, Evangelos Simeonidis, Karin Lanthaler,
906 Pınar Pir, Chuan Lu, et al. 2010. 'Further Developments towards a Genome-Scale
907 Metabolic Model of Yeast'. *BMC Systems Biology* 4 (October): 145.
908 https://doi.org/10.1186/1752-0509-4-145.
909 Esnault, Catherine, Thierry Dulermo, Aleksey Smirnov, Ahmed Askora, Michelle David, Ariane
910 Deniset-Besseau, Ian-Barry Holland, and Marie-Joelle Virolle. 2017. 'Strong Antibiotic
911 Production Is Correlated with Highly Active Oxidative Metabolism in Streptomyces
912 Coelicolor M145'. *Scientific Reports* 7 (1): 200. https://doi.org/10.1038/s41598-017-
913 00259-9.
914 Feist, Adam M., Christopher S. Henry, Jennifer L. Reed, Markus Krummenacker, Andrew R.
915 Joyce, Peter D. Karp, Linda J. Broadbelt, Vassily Hatzimanikatis, and Bernhard Ø
916 Palsson. 2007. 'A Genome-scale Metabolic Reconstruction for Escherichia Coli K-12
917 MG1655 That Accounts for 1260 ORFs and Thermodynamic Information'. *Molecular*
918 *Systems Biology* 3 (1): 121. https://doi.org/10.1038/msb4100155.
919 Fink, D., N. Weißschuh, J. Reuther, W. Wohlleben, and A. Engels. 2002. 'Two Transcriptional
920 Regulators GlnR and GlnRII Are Involved in Regulation of Nitrogen Metabolism in
921 *Streptomyces Coelicolor* A3(2)'. *Molecular Microbiology* 46 (2): 331–47.
922 https://doi.org/10.1046/j.1365-2958.2002.03150.x.
923 Flamholz, Avi, Elad Noor, Arren Bar-Even, and Ron Milo. 2012. 'EQuilibrator—the Biochemical
924 Thermodynamics Calculator'. *Nucleic Acids Research* 40 (D1): D770–75.
925 https://doi.org/10.1093/nar/gkr874.

926 Gaal, Tamas, Michael S. Bartlett, Wilma Ross, Charles L. Turnbough, and Richard L. Gourse.
927 1997. 'Transcription Regulation by Initiating NTP Concentration: RRNA Synthesis in
928 Bacteria'. *Science* 278 (5346): 2092–97.
929 https://doi.org/10.1126/science.278.5346.2092.
930 Gallo, Giuseppe, Giovanni Renzone, Rosa Alduina, Efthimia Stegmann, Tilmann Weber, Anna
931 Eliasson Lantz, Jette Thykaer, Fabio Sangiorgi, Andrea Scaloni, and Anna Maria Puglia.
932 2010. 'Differential Proteomic Analysis Reveals Novel Links between Primary
933 Metabolism and Antibiotic Production in Amycolatopsis Balhimycina'. *PROTEOMICS* 10
934 (7): 1336–58. https://doi.org/10.1002/pmic.200900175.
935 Getsin, Ilya, Gina H Nalbandian, Daniel C Yee, Ake Vastermark, Philipp CG Paparoditis, Vamsee
936 S Reddy, and Milton H Saier. 2013. 'Comparative Genomics of Transport Proteins in
937 Developmental Bacteria: Myxococcus Xanthus and Streptomyces Coelicolor'. *BMC*
938 *Microbiology* 13 (December): 279. https://doi.org/10.1186/1471-2180-13-279.
939 Gomez-Escribano, Juan Pablo, and Mervyn J. Bibb. 2011. 'Engineering Streptomyces Coelicolor
940 for Heterologous Expression of Secondary Metabolite Gene Clusters'. *Microbial*
941 *Biotechnology* 4 (2): 207–15. https://doi.org/10.1111/j.1751-7915.2010.00219.x.
942 ———. 2014. 'Heterologous Expression of Natural Product Biosynthetic Gene Clusters in
943 Streptomyces Coelicolor: From Genome Mining to Manipulation of Biosynthetic
944 Pathways'. *Journal of Industrial Microbiology & Biotechnology* 41 (2): 425–31.
945 https://doi.org/10.1007/s10295-013-1348-5.
946 Gomez-Escribano, Juan Pablo, Lijiang Song, David J. Fox, Valerie Yeo, Mervyn J. Bibb, and
947 Gregory L. Challis. 2012. 'Structure and Biosynthesis of the Unusual Polyketide Alkaloid
948 Coelimycin P1, a Metabolic Product of the Cpk Gene Cluster of Streptomyces Coelicolor
949 M145'. *Chemical Science* 3 (9): 2716–20. https://doi.org/10.1039/C2SC20410J.

950 Gu, Changdai, Gi Bae Kim, Won Jun Kim, Hyun Uk Kim, and Sang Yup Lee. 2019. 'Current Status
951 and Applications of Genome-Scale Metabolic Models'. *Genome Biology* 20 (1): 121.
952 https://doi.org/10.1186/s13059-019-1730-3.
953 Hahn, Ji-Sook, So-Young Oh, and Jung-Hye Roe. 2002. 'Role of OxyR as a Peroxide-Sensing
954 Positive Regulator in Streptomyces Coelicolor A3(2)'. *Journal of Bacteriology* 184 (19):
955 5214–22. https://doi.org/10.1128/JB.184.19.5214-5222.2002.
956 Hastings, Janna, Gareth Owen, Adriano Dekker, Marcus Ennis, Namrata Kale, Venkatesh
957 Muthukrishnan, Steve Turner, Neil Swainston, Pedro Mendes, and Christoph
958 Steinbeck. 2016. 'ChEBI in 2016: Improved Services and an Expanding Collection of
959 Metabolites'. *Nucleic Acids Research* 44 (D1): D1214–19.
960 https://doi.org/10.1093/nar/gkv1031.
961 Heavner, Benjamin D., Kieran Smallbone, Brandon Barker, Pedro Mendes, and Larry P. Walker.
962 2012. 'Yeast 5 – an Expanded Reconstruction of the Saccharomyces Cerevisiae
963 Metabolic Network'. *BMC Systems Biology* 6 (1): 55. https://doi.org/10.1186/1752-
964 0509-6-55.
965 Heavner, Benjamin D., Kieran Smallbone, Nathan D. Price, and Larry P. Walker. 2013. 'Version
966 6 of the Consensus Yeast Metabolic Network Refines Biochemical Coverage and
967 Improves Model Performance'. *Database: The Journal of Biological Databases and*
968 *Curation* 2013: bat059. https://doi.org/10.1093/database/bat059.
969 Hefzi, Hooman, Kok Siong Ang, Michael Hanscho, Aarash Bordbar, David Ruckerbauer,
970 Meiyappan Lakshmanan, Camila A. Orellana, et al. 2016. 'A Consensus Genome-Scale
971 Reconstruction of Chinese Hamster Ovary Cell Metabolism'. *Cell Systems* 3 (5): 434-
972 443.e8. https://doi.org/10.1016/j.cels.2016.10.020.

973 Herrgård, Markus J., Neil Swainston, Paul Dobson, Warwick B. Dunn, K. Yalçin Arga, Mikko
974 Arvas, Nils Blüthgen, et al. 2008. 'A Consensus Yeast Metabolic Network
975 Reconstruction Obtained from a Community Approach to Systems Biology'. *Nature*
976 *Biotechnology* 26 (10): 1155–60. https://doi.org/10.1038/nbt1492.
977 Hesketh, Andrew, Wenqiong Joan Chen, Jamie Ryding, Sherman Chang, and Mervyn Bibb.
978 2007. 'The Global Role of PpGpp Synthesis in Morphological Differentiation and
979 Antibiotic Production in Streptomyces Coelicolor A3(2)'. *Genome Biology* 8 (8): R161.
980 https://doi.org/10.1186/gb-2007-8-8-r161.
981 Hopwood, David A. 2007. *Streptomyces in Nature and Medicine: The Antibiotic Makers*. USA:
982 Oxford University Press.
983 Horinouchi, Sueharu. 2003. 'AfsR as an Integrator of Signals That Are Sensed by Multiple
984 Serine/Threonine Kinases in Streptomyces Coelicolor A3(2)'. *Journal of Industrial*
985 *Microbiology and Biotechnology* 30 (8): 462–67. https://doi.org/10.1007/s10295-003-
986 0063-z.
987 Hu, Haifeng, Qin Zhang, and Kozo Ochi. 2002. 'Activation of Antibiotic Biosynthesis by
988 Specified Mutations in the RpoB Gene (Encoding the RNA Polymerase β Subunit) of
989 Streptomyces Lividans'. *Journal of Bacteriology* 184 (14): 3984–91.
990 https://doi.org/10.1128/JB.184.14.3984-3991.2002.
991 Hutchings, Matthew I., Paul A. Hoskisson, Govind Chandra, and Mark J. Buttner. 2004. 'Sensing
992 and Responding to Diverse Extracellular Signals? Analysis of the Sensor Kinases and
993 Response Regulators of Streptomyces Coelicolor A3(2)'. *Microbiology,* 150 (9): 2795–
994 2806. https://doi.org/10.1099/mic.0.27181-0.

995 Jäger, G., F. Battke, and K. Nieselt. 2011. 'TIALA — Time Series Alignment Analysis'. In *2011*
996 *IEEE Symposium on Biological Data Visualization (BioVis).*, 55–61.
997 https://doi.org/10.1109/BioVis.2011.6094048.
998 Jones, Greg, Ricardo Del Sol, Ed Dudley, and Paul Dyson. 2011. 'Forkhead-Associated Proteins
999 Genetically Linked to the Serine/Threonine Kinase PknB Regulate Carbon Flux towards
1000 Antibiotic Biosynthesis in Streptomyces Coelicolor'. *Microbial Biotechnology* 4 (2):
1001 263–74. https://doi.org/10.1111/j.1751-7915.2010.00237.x.
1002 Jonsbu, E., B. Christensen, and J. Nielsen. 2001. 'Changes of in Vivo Fluxes through Central
1003 Metabolic Pathways during the Production of Nystatin by Streptomyces Noursei in
1004 Batch Culture'. *Applied Microbiology and Biotechnology* 56 (1): 93–100.
1005 https://doi.org/10.1007/s002530100613.
1006 Kanehisa, M. 2000. 'KEGG: Kyoto Encyclopedia of Genes and Genomes'. *Nucleic Acids Research*
1007 28 (1): 27–30. https://doi.org/10.1093/nar/28.1.27.
1008 Kanehisa, Minoru, Yoko Sato, Miho Furumichi, Kanae Morishima, and Mao Tanabe. 2019.
1009 'New Approach for Understanding Genome Variations in KEGG'. *Nucleic Acids Research*
1010 47 (D1): D590–95. https://doi.org/10.1093/nar/gky962.
1011 Karp, Peter D., Richard Billington, Ron Caspi, Carol A. Fulcher, Mario Latendresse, Anamika
1012 Kothari, Ingrid M. Keseler, et al. 2017. 'The BioCyc Collection of Microbial Genomes
1013 and Metabolic Pathways'. *Briefings in Bioinformatics*, August.
1014 https://doi.org/10.1093/bib/bbx085.
1015 Kepplinger, Bernhard, Stephanie Morton-Laing, Kenneth Holst Seistrup, Emma Claire Louise
1016 Marrs, Adam Paul Hopkins, John David Perry, Henrik Strahl, Michael John Hall, Jeff
1017 Errington, and Nicholas Edward Ellis Allenby. 2018. 'Mode of Action and Heterologous

1018 Expression of the Natural Product Antibiotic Vancoresmycin'. *ACS Chemical Biology* 13
1019 (1): 207–14. https://doi.org/10.1021/acschembio.7b00733.
1020 Kieser, Tobias, Mervyn J Bibb, Mark J Buttner, Keith F Chater, and David A Hopwood. 2000.
1021 *Practical Streptomyces Genetics*. Vol. 291. Norwich, UK: John Innes Foundation.
1022 Kim, Dong-Jin, Jung-Hyun Huh, Young-Yell Yang, Choong-Min Kang, In-Hyung Lee, Chang-Gu
1023 Hyun, Soon-Kwang Hong, and Joo-Won Suh. 2003. 'Accumulation of S-Adenosyl-l-
1024 Methionine Enhances Production of Actinorhodin but Inhibits Sporulation in
1025 Streptomyces Lividans TK23'. *Journal of Bacteriology* 185 (2): 592–600.
1026 https://doi.org/10.1128/JB.185.2.592-600.2003.
1027 Kim, Minsuk Woo, Jeong Sang Yi, Ji-Nu Joonwon Ji-Nu Nu Joonwon Kim, Ji-Nu Joonwon Ji-Nu
1028 Nu Joonwon Kim, Minsuk Woo Kim, and Byung-Gee Gee Kim. 2014. 'Reconstruction of
1029 a High-Quality Metabolic Model Enables the Identification of Gene Overexpression
1030 Targets for Enhanced Antibiotic Production in Streptomyces Coelicolor A3(2)'.
1031 *Biotechnology Journal* 9 (9): 1185–94. https://doi.org/10.1002/biot.201300539.
1032 King, Zachary A., Andreas Dräger, Ali Ebrahim, Nikolaus Sonnenschein, Nathan E. Lewis, and
1033 Bernhard O. Palsson. 2015. 'Escher: A Web Application for Building, Sharing, and
1034 Embedding Data-Rich Visualizations of Biological Pathways'. *PLOS Computational*
1035 *Biology* 11 (8): e1004321. https://doi.org/10.1371/journal.pcbi.1004321.
1036 King, Zachary A., Justin Lu, Andreas Dräger, Philip Miller, Stephen Federowicz, Joshua A.
1037 Lerman, Ali Ebrahim, Bernhard O. Palsson, Nathan E. Lewis, and Hastings J. 2016. 'BiGG
1038 Models: A Platform for Integrating, Standardizing and Sharing Genome-Scale Models'.
1039 *Nucleic Acids Research* 44 (D1): D515–22. https://doi.org/10.1093/nar/gkv1049.
1040 Kumelj, Tjaša, Snorre Sulheim, Alexander Wentzel, and Eivind Almaas. 2018. 'Predicting Strain
1041 Engineering Strategies Using IKS1317: A Genome-Scale Metabolic Model of

1042 Streptomyces Coelicolor'. *Biotechnology Journal* 0 (0): 1800180.
1043 https://doi.org/10.1002/biot.201800180.
1044 Lamb, David C., Haruo Ikeda, David R. Nelson, Jun Ishikawa, Tove Skaug, Colin Jackson, Satoshi
1045 Omura, Michael R. Waterman, and Steven L. Kelly. 2003. 'Cytochrome P450
1046 Complement (CYPome) of the Avermectin-Producer Streptomyces Avermitilis and
1047 Comparison to That of Streptomyces Coelicolor A3(2)'. *Biochemical and Biophysical*
1048 *Research Communications* 307 (3): 610–19. https://doi.org/10.1016/S0006-
1049 291X(03)01231-2.
1050 Latifi, Amel, Marion Ruiz, and Cheng-Cai Zhang. 2009. 'Oxidative Stress in Cyanobacteria'.
1051 *FEMS Microbiology Reviews* 33 (2): 258–78. https://doi.org/10.1111/j.1574-
1052 6976.2008.00134.x.
1053 Lee, Ping-Chin, Takashi Umeyama, and Sueharu Horinouchi. 2002. 'AfsS Is a Target of AfsR, a
1054 Transcriptional Factor with ATPase Activity That Globally Controls Secondary
1055 Metabolism in Streptomyces Coelicolor A3(2)'. *Molecular Microbiology* 43 (6): 1413–
1056 30. https://doi.org/10.1046/j.1365-2958.2002.02840.x.
1057 Li, Lei, Weihong Jiang, and Yinhua Lu. 2017. 'A Novel Two-Component System, GluR-GluK,
1058 Involved in Glutamate Sensing and Uptake in Streptomyces Coelicolor'. *Journal of*
1059 *Bacteriology* 199 (18). https://doi.org/10.1128/JB.00097-17.
1060 Li, Tong, Yuanyuan Du, Qiu Cui, Jingtao Zhang, Weiming Zhu, Kui Hong, and Wenli Li. 2013.
1061 'Cloning, Characterization and Heterologous Expression of the Indolocarbazole
1062 Biosynthetic Gene Cluster from Marine-Derived Streptomyces Sanyensis FMA'. *Marine*
1063 *Drugs* 11 (2): 466–88. https://doi.org/10.3390/md11020466.
1064 Li, Xiao, Juan Wang, Shanshan Li, Junjie Ji, Weishan Wang, and Keqian Yang. 2015. 'ScbR- and
1065 ScbR2-Mediated Signal Transduction Networks Coordinate Complex Physiological

1066 Responses in *Streptomyces Coelicolor*'. *Scientific Reports* 5 (October): 14831.
1067 https://doi.org/10.1038/srep14831.
1068 Liao, Yang, Gordon K. Smyth, and Wei Shi. 2014. 'FeatureCounts: An Efficient General Purpose
1069 Program for Assigning Sequence Reads to Genomic Features'. *Bioinformatics (Oxford,*
1070 *England)* 30 (7): 923–30. https://doi.org/10.1093/bioinformatics/btt656.
1071 Licona-Cassani, Cuauhtemoc, Esteban Marcellin, Lake-Ee Quek, Shana Jacob, and Lars K.
1072 Nielsen. 2012. 'Reconstruction of the Saccharopolyspora Erythraea Genome-Scale
1073 Model and Its Use for Enhancing Erythromycin Production'. *Antonie van Leeuwenhoek*
1074 102 (3): 493–502. https://doi.org/10.1007/s10482-012-9783-2.
1075 Lieven, Christian, Moritz Emanuel Beber, Brett G. Olivier, Frank T. Bergmann, Meric Ataman,
1076 Parizad Babaei, Jennifer A. Bartell, et al. 2018. 'Memote: A Community-Driven Effort
1077 towards a Standardized Genome-Scale Metabolic Model Test Suite'. *BioRxiv*, July,
1078 350991. https://doi.org/10.1101/350991.
1079 Liu, Gang, Keith F. Chater, Govind Chandra, Guoqing Niu, and Huarong Tan. 2013. 'Molecular
1080 Regulation of Antibiotic Biosynthesis in Streptomyces'. *Microbiology and Molecular*
1081 *Biology Reviews* 77 (1): 112–43. https://doi.org/10.1128/MMBR.00054-12.
1082 Love, Michael I., Wolfgang Huber, and Simon Anders. 2014. 'Moderated Estimation of Fold
1083 Change and Dispersion for RNA-Seq Data with DESeq2'. *Genome Biology* 15 (12): 550.
1084 https://doi.org/10.1186/s13059-014-0550-8.
1085 Lu, Hongzhong, Feiran Li, Benjamín J. Sánchez, Zhengming Zhu, Gang Li, Iván Domenzain,
1086 Simonas Marcišauskas, et al. 2019. 'A Consensus S. Cerevisiae Metabolic Model Yeast8
1087 and Its Ecosystem for Comprehensively Probing Cellular Metabolism'. *Nature*
1088 *Communications* 10 (1): 1–13. https://doi.org/10.1038/s41467-019-11581-3.

1089 Martín, Juan F. 2004. 'Phosphate Control of the Biosynthesis of Antibiotics and Other
1090 Secondary Metabolites Is Mediated by the PhoR-PhoP System: An Unfinished Story'.
1091 *Journal of Bacteriology* 186 (16): 5197–5201. https://doi.org/10.1128/JB.186.16.5197-
1092 5201.2004.
1093 Martín, Juan F., Antonio Rodríguez-García, and Paloma Liras. 2017. 'The Master Regulator
1094 PhoP Coordinates Phosphate and Nitrogen Metabolism, Respiration, Cell
1095 Differentiation and Antibiotic Biosynthesis: Comparison in *Streptomyces Coelicolor* and
1096 *Streptomyces Avermitilis*'. *The Journal of Antibiotics* 70 (5): 534–41.
1097 https://doi.org/10.1038/ja.2017.19.
1098 Martín, Juan F., Fernando Santos-Beneit, Antonio Rodríguez-García, Alberto Sola-Landa,
1099 Margaret C. M. Smith, Trond E. Ellingsen, Kay Nieselt, Nigel J. Burroughs, and Ellizabeth
1100 M. H. Wellington. 2012. 'Transcriptomic Studies of Phosphate Control of Primary and
1101 Secondary Metabolism in Streptomyces Coelicolor'. *Applied Microbiology and*
1102 *Biotechnology* 95 (1): 61–75. https://doi.org/10.1007/s00253-012-4129-6.
1103 Martín-Martín, Seomara, Antonio Rodríguez-García, Fernando Santos-Beneit, Etelvina Franco-
1104 Domínguez, Alberto Sola-Landa, and Juan Francisco Martín. 2018. 'Self-Control of the
1105 PHO Regulon: The PhoP-Dependent Protein PhoU Controls Negatively Expression of
1106 Genes of PHO Regulon in *Streptomyces Coelicolor*'. *The Journal of Antibiotics* 71 (1):
1107 113–22. https://doi.org/10.1038/ja.2017.130.
1108 Mi, Huaiyu, Anushya Muruganujan, Dustin Ebert, Xiaosong Huang, and Paul D. Thomas. 2019.
1109 'PANTHER Version 14: More Genomes, a New PANTHER GO-Slim and Improvements in
1110 Enrichment Analysis Tools'. *Nucleic Acids Research* 47 (D1): D419–26.
1111 https://doi.org/10.1093/nar/gky1038.

1112 Millan-Oropeza, Aaron, Céline Henry, Mélisande Blein-Nicolas, Anne Aubert-Frambourg, Fathi
1113 Moussa, Jean Bleton, and Marie-Jöelle Virolle. 2017. 'Quantitative Proteomics Analysis
1114 Confirmed Oxidative Metabolism Predominates in Streptomyces Coelicolor versus
1115 Glycolytic Metabolism in Streptomyces Lividans'. *Journal of Proteome Research* 16 (7):
1116 2597–2613. https://doi.org/10.1021/acs.jproteome.7b00163.
1117 Mohite, Omkar S., Tilmann Weber, Hyun Uk Kim, and Sang Yup Lee. 2019. 'Genome-Scale
1118 Metabolic Reconstruction of Actinomycetes for Antibiotics Production'. *Biotechnology*
1119 *Journal* 14 (1): 1800377. https://doi.org/10.1002/biot.201800377.
1120 Moretti, Sébastien, Olivier Martin, T. Van Du Tran, Alan Bridge, Anne Morgat, and Marco
1121 Pagni. 2016. 'MetaNetX/MNXref – Reconciliation of Metabolites and Biochemical
1122 Reactions to Bring Together Genome-Scale Metabolic Networks'. *Nucleic Acids*
1123 *Research* 44 (D1): D523–26. https://doi.org/10.1093/nar/gkv1117.
1124 Naseer, Nawar, Joshua A. Shapiro, and Monica Chander. 2014. 'RNA-Seq Analysis Reveals a
1125 Six-Gene SoxR Regulon in Streptomyces Coelicolor'. *PloS One* 9 (8): e106181.
1126 https://doi.org/10.1371/journal.pone.0106181.
1127 Nepal, Keshav K., and Guojun Wang. 2019. 'Streptomycetes: Surrogate Hosts for the Genetic
1128 Manipulation of Biosynthetic Gene Clusters and Production of Natural Products'.
1129 *Biotechnology Advances* 37 (1): 1–20.
1130 https://doi.org/10.1016/j.biotechadv.2018.10.003.
1131 Nieselt, Kay, Florian Battke, Alexander Herbig, Per Bruheim, Alexander Wentzel, Øyvind M
1132 Jakobsen, Håvard Sletta, et al. 2010. 'The Dynamic Architecture of the Metabolic
1133 Switch in Streptomyces Coelicolor'. *BMC Genomics* 11 (1): 10.
1134 https://doi.org/10.1186/1471-2164-11-10.

1135 Nothaft, Harald, Sébastien Rigali, Bart Boomsma, Magdalena Swiatek, Kenneth J. McDowall,
1136 Gilles P van Wezel, and Fritz Titgemeyer. 2010. 'The Permease Gene NagE2 Is the Key
1137 to N-Acetylglucosamine Sensing and Utilization in Streptomyces Coelicolor and Is
1138 Subject to Multi-Level Control'. *Molecular Microbiology* 75 (5): 1133–44.
1139 https://doi.org/10.1111/j.1365-2958.2009.07020.x.
1140 Okamoto, Susumu, Alexander Lezhava, Takeshi Hosaka, Yoshiko Okamoto-Hosoya, and Kozo
1141 Ochi. 2003. 'Enhanced Expression of S-Adenosylmethionine Synthetase Causes
1142 Overproduction of Actinorhodin in Streptomyces Coelicolor A3(2)'. *Journal of*
1143 *Bacteriology* 185 (2): 601–9. https://doi.org/10.1128/JB.185.2.601-609.2003.
1144 Orth, Jeffrey D, Ines Thiele, and Bernhard Ø O Palsson. 2010. 'What Is Flux Balance Analysis?'
1145 *Nat Biotech* 28 (3): 245–48. https://doi.org/10.1038/nbt.1614.
1146 Perez-Riverol, Yasset, Attila Csordas, Jingwen Bai, Manuel Bernal-Llinares, Suresh
1147 Hewapathirana, Deepti J. Kundu, Avinash Inuganti, et al. 2019. 'The PRIDE Database
1148 and Related Tools and Resources in 2019: Improving Support for Quantification Data'.
1149 *Nucleic Acids Research* 47 (D1): D442–50. https://doi.org/10.1093/nar/gky1106.
1150 Rigali, Sébastien, Fritz Titgemeyer, Sharief Barends, Suzanne Mulder, Andreas W Thomae,
1151 David A Hopwood, and Gilles P van Wezel. 2008. 'Feast or Famine: The Global
1152 Regulator DasR Links Nutrient Stress to Antibiotic Production by Streptomyces'. *EMBO*
1153 *Reports* 9 (7): 670–75. https://doi.org/10.1038/embor.2008.83.
1154 Robinson, Jonathan L., and Jens Nielsen. 2016. 'Integrative Analysis of Human Omics Data
1155 Using Biomolecular Networks'. *Molecular BioSystems* 12 (10): 2953–64.
1156 https://doi.org/10.1039/c6mb00476h.
1157 Rodriguez, Eduardo, Laura Navone, Paula Casati, and Hugo Gramajo. 2012. 'Impact of Malic
1158 Enzymes on Antibiotic and Triacylglycerol Production in Streptomyces Coelicolor'.

1159 *Applied and Environmental Microbiology* 78 (13): 4571–79.
1160 https://doi.org/10.1128/AEM.00838-12.
1161 Rutledge, Peter J., and Gregory L. Challis. 2015. 'Discovery of Microbial Natural Products by
1162 Activation of Silent Biosynthetic Gene Clusters'. *Nature Reviews Microbiology* 13 (8):
1163 509–23. https://doi.org/10.1038/nrmicro3496.
1164 Sánchez, Benjamín J., Cheng Zhang, Avlant Nilsson, Petri-Jaan Lahtvee, Eduard J. Kerkhoven,
1165 and Jens Nielsen. 2017. 'Improving the Phenotype Predictions of a Yeast Genome-scale
1166 Metabolic Model by Incorporating Enzymatic Constraints'. *Molecular Systems Biology*
1167 13 (8): 935. https://doi.org/10.15252/msb.20167411.
1168 Shin, Jung-Ho, Atul K. Singh, Dong-Joo Cheon, and Jung-Hye Roe. 2011. 'Activation of the SoxR
1169 Regulon in Streptomyces Coelicolor by the Extracellular Form of the Pigmented
1170 Antibiotic Actinorhodin'. *Journal of Bacteriology* 193 (1): 75–81.
1171 https://doi.org/10.1128/JB.00965-10.
1172 Smirnov, Aleksey, Catherine Esnault, Magali Prigent, Ian Barry Holland, and Marie-Joelle
1173 Virolle. 2015. 'Phosphate Homeostasis in Conditions of Phosphate Proficiency and
1174 Limitation in the Wild Type and the PhoP Mutant of Streptomyces Lividans'. *PLoS ONE*
1175 10 (5). https://doi.org/10.1371/journal.pone.0126221.
1176 Sola-Landa, A., R. S. Moura, and J. F. Martín. 2003. 'The Two-Component PhoR-PhoP System
1177 Controls Both Primary Metabolism and Secondary Metabolite Biosynthesis in
1178 Streptomyces Lividans'. *Proceedings of the National Academy of Sciences of the United*
1179 *States of America* 100 (10): 6133–38. https://doi.org/10.1073/pnas.0931429100.
1180 Sola-Landa, Alberto, Antonio Rodríguez-García, Etelvina Franco-Domínguez, and Juan F.
1181 Martín. 2005. 'Binding of PhoP to Promoters of Phosphate-Regulated Genes in

1182 Streptomyces Coelicolor: Identification of PHO Boxes'. *Molecular Microbiology* 56 (5):
1183 1373–85. https://doi.org/10.1111/j.1365-2958.2005.04631.x.
1184 Srivatsan, Anjana, and Jue D Wang. 2008. 'Control of Bacterial Transcription, Translation and
1185 Replication by (p)PpGpp'. *Current Opinion in Microbiology*, Cell Regulation, 11 (2): 100–
1186 105. https://doi.org/10.1016/j.mib.2008.02.001.
1187 Stahl, Wilhelm, and Helmut Sies. 2003. 'Antioxidant Activity of Carotenoids'. *Molecular*
1188 *Aspects of Medicine*, Fat Soluble Vitamins: Old Molecules with Novel Properties, 24 (6):
1189 345–51. https://doi.org/10.1016/S0098-2997(03)00030-X.
1190 Stirrett, Karen, Claudio Denoya, and Janet Westpheling. 2009. 'Branched-Chain Amino Acid
1191 Catabolism Provides Precursors for the Type II Polyketide Antibiotic, Actinorhodin, via
1192 Pathways That Are Nutrient Dependent'. *Journal of Industrial Microbiology &*
1193 *Biotechnology* 36 (1): 129–37. https://doi.org/10.1007/s10295-008-0480-0.
1194 Thanapipatsiri, Anyarat, Jan Claesen, Juan-Pablo Gomez-Escribano, Mervyn Bibb, and Arinthip
1195 Thamchaipenet. 2015. 'A Streptomyces Coelicolor Host for the Heterologous
1196 Expression of Type III Polyketide Synthase Genes'. *Microbial Cell Factories* 14
1197 (September). https://doi.org/10.1186/s12934-015-0335-0.
1198 The UniProt Consortium. 2019. 'UniProt: A Worldwide Hub of Protein Knowledge'. *Nucleic*
1199 *Acids Research* 47 (D1): D506–15. https://doi.org/10.1093/nar/gky1049.
1200 The Gene Ontology Consortium. 2019. 'The Gene Ontology Resource: 20 Years and Still GOing
1201 Strong'. *Nucleic Acids Research* 47 (D1): D330–38.
1202 https://doi.org/10.1093/nar/gky1055.
1203 Thiele, Ines, and Bernhard Ø Palsson. 2010. 'A Protocol for Generating a High-Quality Genome-
1204 Scale Metabolic Reconstruction.' *Nature Protocols* 5 (1): 93–121.
1205 https://doi.org/10.1038/nprot.2009.203.

1206 Thiele, Ines, Neil Swainston, Ronan M T Fleming, Andreas Hoppe, Swagatika Sahoo, Maike K
1207 Aurich, Hulda Haraldsdottir, et al. 2013. 'A Community-Driven Global Reconstruction
1208 of Human Metabolism'. *Nature Biotechnology* 31 (5).
1209 https://doi.org/10.1038/nbt.2488.
1210 Thomas, Louise, David A Hodgson, Alexander Wentzel, Kay Nieselt, Trond E Ellingsen, Jonathan
1211 Moore, Edward R Morrissey, et al. 2012. 'Metabolic Switches and Adaptations
1212 Deduced from the Proteomes of Streptomyces Coelicolor Wild Type and PhoP Mutant
1213 Grown in Batch Culture.' *Molecular & Cellular Proteomics : MCP* 11 (2): M111.013797.
1214 https://doi.org/10.1074/mcp.M111.013797.
1215 Toro, León, Laura Pinilla, Claudio Avignone-Rossa, and Rigoberto Ríos-Estepa. 2018. 'An
1216 Enhanced Genome-Scale Metabolic Reconstruction of Streptomyces Clavuligerus
1217 Identifies Novel Strain Improvement Strategies'. *Bioprocess and Biosystems*
1218 *Engineering* 41 (5): 657–69. https://doi.org/10.1007/s00449-018-1900-9.
1219 Valton, Julien, Carole Mathevon, Marc Fontecave, Vincent Nivière, and David P. Ballou. 2008.
1220 'Mechanism and Regulation of the Two-Component FMN-Dependent Monooxygenase
1221 ActVA-ActVB from Streptomyces Coelicolor'. *The Journal of Biological Chemistry* 283
1222 (16): 10287–96. https://doi.org/10.1074/jbc.M709730200.
1223 Valverde, José R., Sonia Gullón, and Rafael P. Mellado. 2018. 'Modelling the Metabolism of
1224 Protein Secretion through the Tat Route in Streptomyces Lividans'. *BMC Microbiology*
1225 18 (1): 59. https://doi.org/10.1186/s12866-018-1199-3.
1226 Wang, Hao, Simonas Marcišauskas, Benjamín J. Sánchez, Iván Domenzain, Daniel Hermansson,
1227 Rasmus Agren, Jens Nielsen, and Eduard J. Kerkhoven. 2018. 'RAVEN 2.0: A Versatile
1228 Toolbox for Metabolic Network Reconstruction and a Case Study on Streptomyces

1229 Coelicolor'. *PLOS Computational Biology* 14 (10): e1006541.
1230 https://doi.org/10.1371/journal.pcbi.1006541.
1231 Wentzel, Alexander, Per Bruheim, Anders Øverby, Øyvind M Jakobsen, Håvard Sletta, Walid A
1232 M Omara, David A Hodgson, and Trond E Ellingsen. 2012. 'Optimized Submerged Batch
1233 Fermentation Strategy for Systems Scale Studies of Metabolic Switching in
1234 Streptomyces Coelicolor A3(2).' *BMC Systems Biology* 6 (June): 59.
1235 https://doi.org/10.1186/1752-0509-6-59.
1236 Wentzel, Alexander, Havard Sletta, Stream Consortium, Trond E. Ellingsen, and Per Bruheim.
1237 2012. 'Intracellular Metabolite Pool Changes in Response to Nutrient Depletion
1238 Induced Metabolic Switching in Streptomyces Coelicolor'. *Metabolites* 2 (1): 178–94.
1239 https://doi.org/10.3390/metabo2010178.
1240 Xu, J., Y. Tozawa, C. Lai, H. Hayashi, and K. Ochi. 2002. 'A Rifampicin Resistance Mutation in
1241 the RpoB Gene Confers PpGpp-Independent Antibiotic Production in Streptomyces
1242 Coelicolor A3(2)'. *Molecular Genetics and Genomics* 268 (2): 179–89.
1243 https://doi.org/10.1007/s00438-002-0730-1.
1244 Yin, Jia, Michael Hoffmann, Xiaoying Bian, Qiang Tu, Fu Yan, Liqiu Xia, Xuezhi Ding, et al. 2015.
1245 'Direct Cloning and Heterologous Expression of the Salinomycin Biosynthetic Gene
1246 Cluster from Streptomyces Albus DSM41398 in Streptomyces Coelicolor A3(2)'.
1247 *Scientific Reports* 5 (1): 15081. https://doi.org/10.1038/srep15081.
1248 Yoshida, Masasuke, Eiro Muneyuki, and Toru Hisabori. 2001. 'ATP Synthase — a Marvellous
1249 Rotary Engine of the Cell'. *Nature Reviews Molecular Cell Biology* 2 (9): 669–77.
1250 https://doi.org/10.1038/35089509.
1251 Zangar, Richard C., Dmitri R. Davydov, and Seema Verma. 2004. 'Mechanisms That Regulate
1252 Production of Reactive Oxygen Species by Cytochrome P450'. *Toxicology and Applied*

Pharmacology, Mechanisms Regulating Enzymes Involved in Xenobiotic Disposition: A Tribute to Ed Bresnick, 199 (3): 316–31. https://doi.org/10.1016/j.taap.2004.01.018.

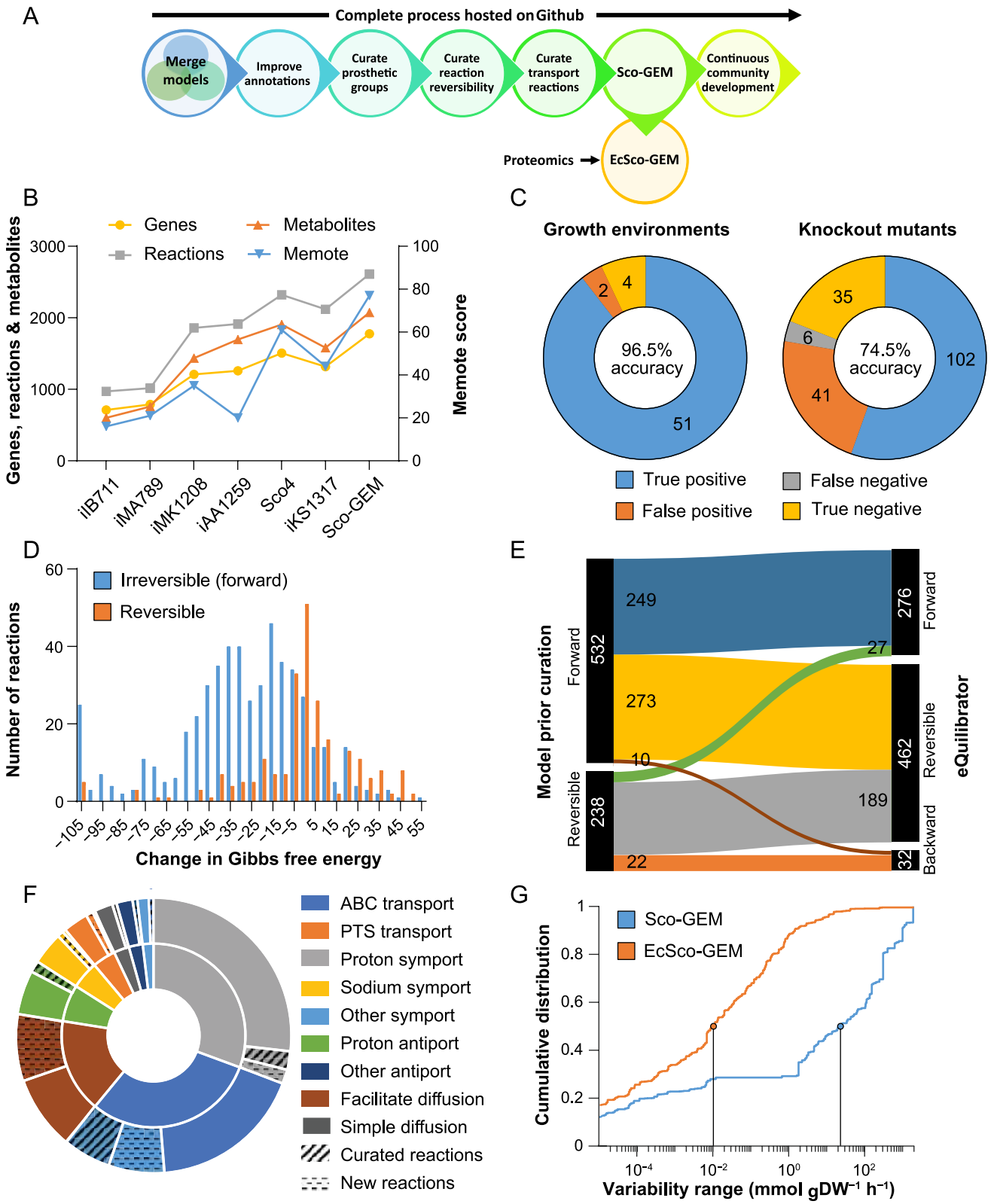
A
Complete process hosted on Github
Merge models
Improve annotations
Curate prosthetic groups
Curate reaction reversibility
Curate transport reactions
Sco-GEM
Continuous community development
Proteomics
EcSco-GEM
B
Genes
Metabolites
Reactions
Memote
Genes, reactions & metabolites
Memote score
iIB711
iMA789
iMK1208
iAA1259
Sco4
iKS1317
Sco-GEM
C
Growth environments
Knockout mutants
96.5% accuracy
74.5% accuracy
True positive
False positive
False negative
True negative
D
Irreversible (forward)
Reversible
Number of reactions
Change in Gibbs free energy
E
Model prior curation
eQuilibrator
Forward
Reversible
Backward
F
ABC transport
PTS transport
Proton symport
Sodium symport
Other symport
Proton antiport
Other antiport
Facilitate diffusion
Simple diffusion
Curated reactions
New reactions
G
Sco-GEM
EcSco-GEM
Cumulative distribution
Variability range (mmol gDW⁻¹ h⁻¹)

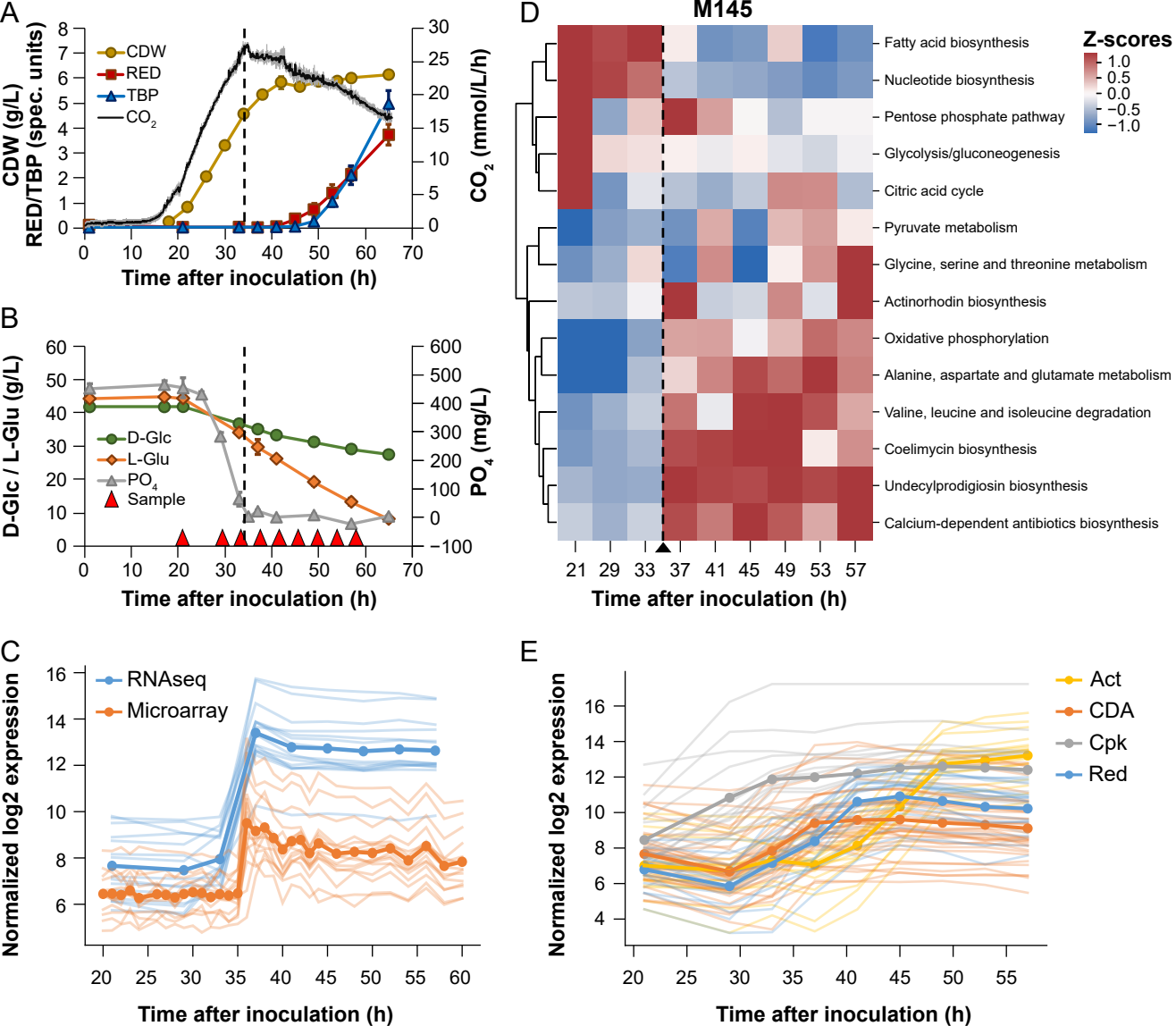
A
CDW
RED
TBP
CO_2
CDW (g/L)
RED/TBP (spec. units)
CO_2 (mmol/L/h)
Time after inoculation (h)
B
D-Glc
L-Glu
PO_4
Sample
D-Glc / L-Glu (g/L)
PO_4 (mg/L)
Time after inoculation (h)
D
M145
Z-scores
Fatty acid biosynthesis
Nucleotide biosynthesis
Pentose phosphate pathway
Glycolysis/gluconeogenesis
Citric acid cycle
Pyruvate metabolism
Glycine, serine and threonine metabolism
Actinorhodin biosynthesis
Oxidative phosphorylation
Alanine, aspartate and glutamate metabolism
Valine, leucine and isoleucine degradation
Coelimycin biosynthesis
Undecylprodigiosin biosynthesis
Calcium-dependent antibiotics biosynthesis
Time after inoculation (h)
C
RNAseq
Microarray
Normalized log2 expression
Time after inoculation (h)
E
Act
CDA
Cpk
Red
Normalized log2 expression
Time after inoculation (h)

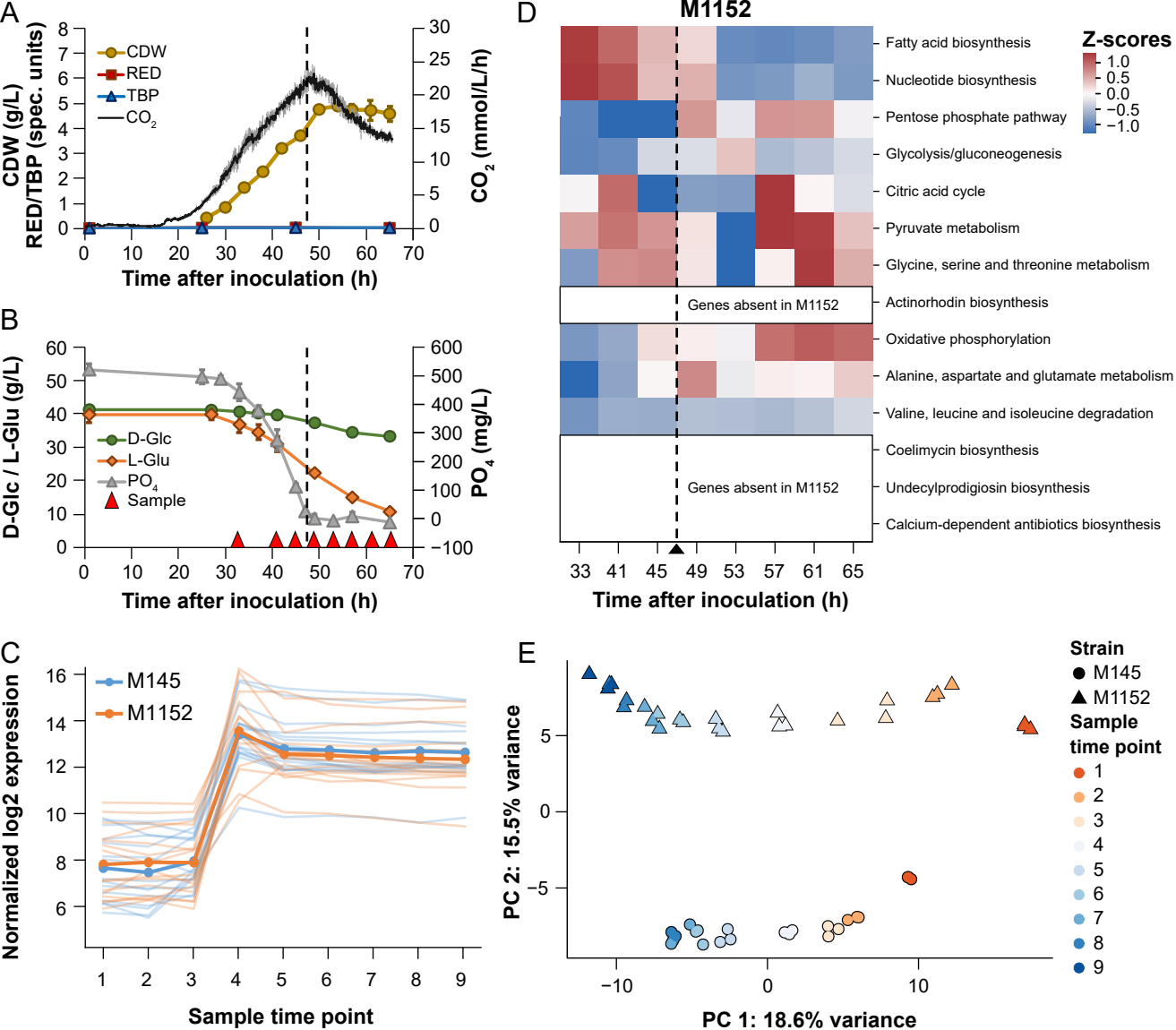
A
CDW
RED
TBP
CO_2
CDW (g/L)
RED/TBP (spec. units)
CO_2 (mmol/L/h)
Time after inoculation (h)
B
D-Glc
L-Glu
PO_4
Sample
D-Glc / L-Glu (g/L)
PO_4 (mg/L)
Time after inoculation (h)
D
M1152
Fatty acid biosynthesis
Nucleotide biosynthesis
Pentose phosphate pathway
Glycolysis/gluconeogenesis
Citric acid cycle
Pyruvate metabolism
Glycine, serine and threonine metabolism
Genes absent in M1152
Actinorhodin biosynthesis
Oxidative phosphorylation
Alanine, aspartate and glutamate metabolism
Valine, leucine and isoleucine degradation
Coelimycin biosynthesis
Genes absent in M1152
Undecylprodigiosin biosynthesis
Calcium-dependent antibiotics biosynthesis
Z-scores
Time after inoculation (h)
C
M145
M1152
Normalized log2 expression
Sample time point
E
Strain
M145
M1152
Sample time point
PC 2: 15.5% variance
PC 1: 18.6% variance

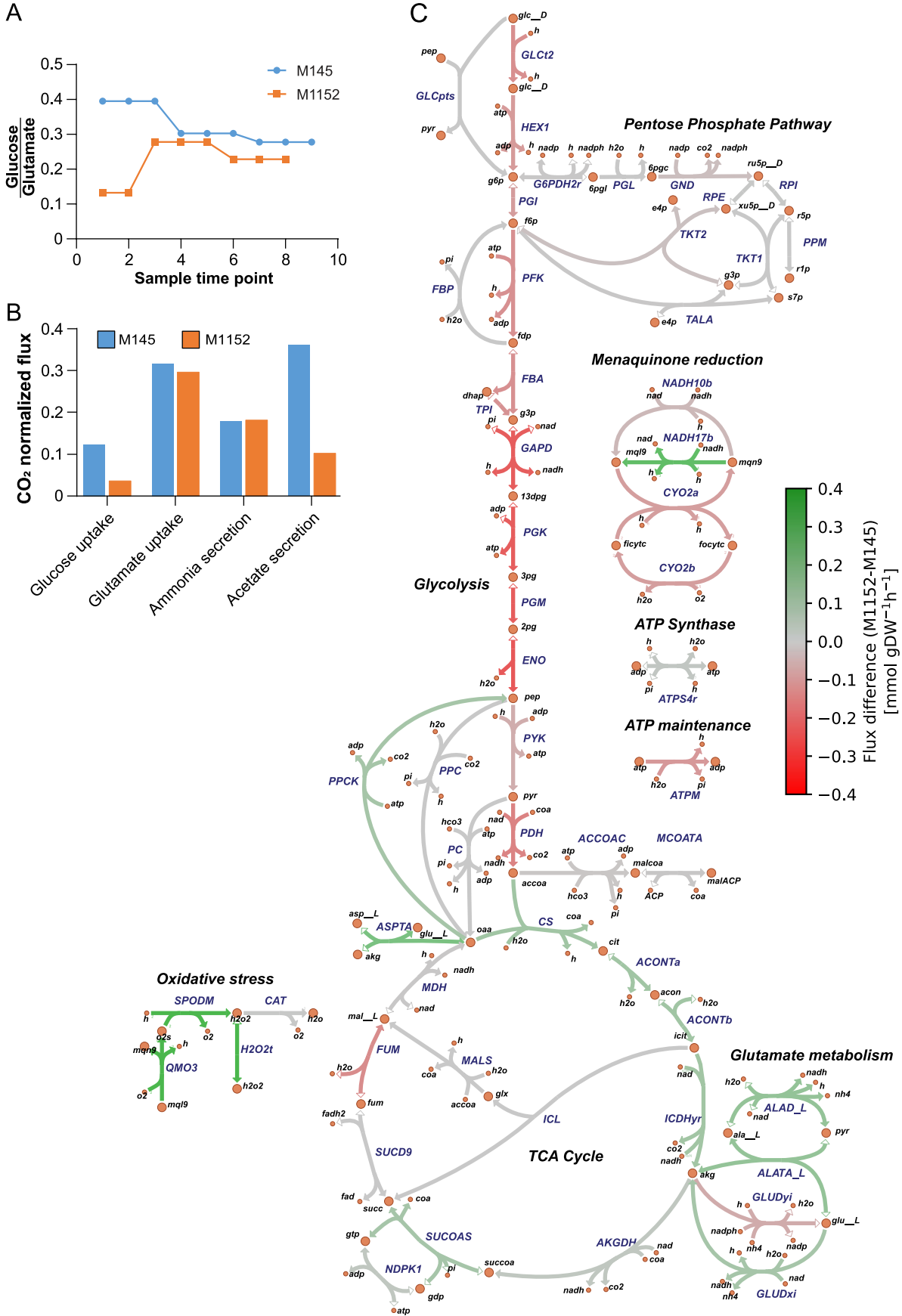
A
Glucose / Glutamate
M145
M1152
Sample time point
B
CO₂ normalized flux
M145
M1152
Glucose uptake
Glutamate uptake
Ammonia secretion
Acetate secretion
C
Pentose Phosphate Pathway
Menaquinone reduction
Glycolysis
ATP Synthase
ATP maintenance
Oxidative stress
Glutamate metabolism
TCA Cycle
Flux difference (M1152-M145)
[mmol gDW⁻¹h⁻¹]

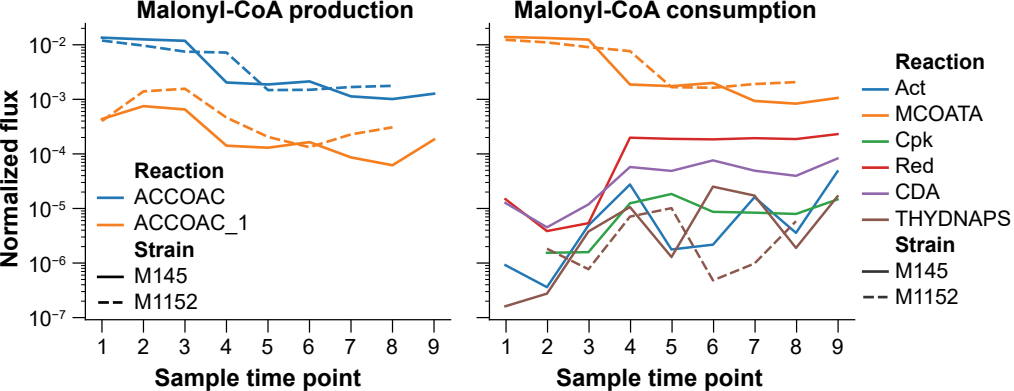
Malonyl-CoA production
Malonyl-CoA consumption
Normalized flux
10^{-2}
10^{-3}
10^{-4}
10^{-5}
10^{-6}
10^{-7}
1 2 3 4 5 6 7 8 9
Sample time point
Reaction
ACCOAC
ACCOAC_1
Strain
M145
M1152
Reaction
Act
MCOATA
Cpk
Red
CDA
THYDNAPS
Strain
M145
M1152

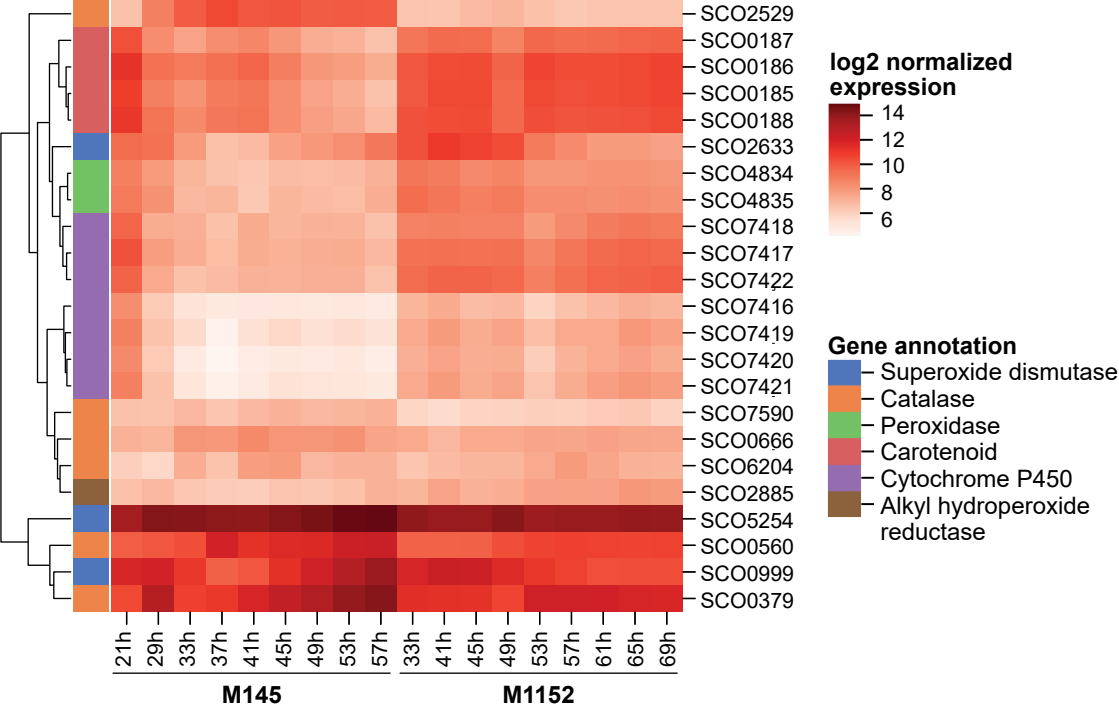
SCO2529
SCO0187
SCO0186
SCO0185
SCO0188
SCO2633
SCO4834
SCO4835
SCO7418
SCO7417
SCO7422
SCO7416
SCO7419
SCO7420
SCO7421
SCO7590
SCO0666
SCO6204
SCO2885
SCO5254
SCO0560
SCO0999
SCO0379
21h
29h
33h
37h
41h
45h
49h
53h
57h
33h
41h
45h
49h
53h
57h
61h
65h
69h
M145
M1152
log2 normalized expression
14
12
10
8
6
Gene annotation
Superoxide dismutase
Catalase
Peroxidase
Carotenoid
Cytochrome P450
Alkyl hydroperoxide reductase

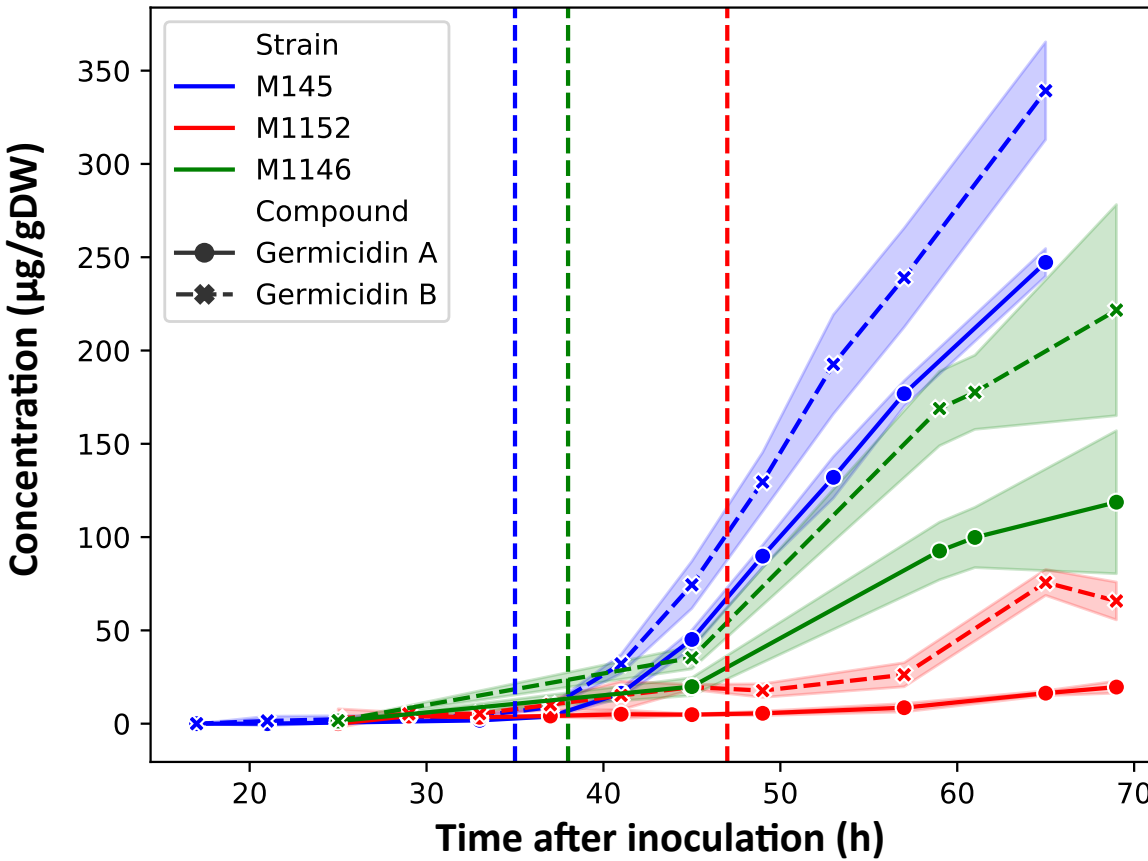
Strain
M145
M1152
M1146
Compound
Germicidin A
Germicidin B
Concentration (µg/gDW)
Time after inoculation (h)
0
50
100
150
200
250
300
350
20
30
40
50
60
70